2.2 One-dimensional nanosystems

John Buckeridge and Alexey A. Sokol

University College London, Kathleen Lonsdale Materials Chemistry, Department of Chemistry, 20 Gordon Street, London WC1H 0AJ, United Kingdom

E-mails: j.buckeridge@ucl.ac.uk, a.sokol@ucl.ac.uk

2.1 Introduction

The simplest example of matter, self-organised at nanoscale, rather than individual nanoparticles considered in the previous chapter, is provided by quasi one-dimensional (1D) objects such as nanowires, rods, ribbons or tubes. The key feature of these systems is the contrast between the confinement of the constituent electrons, and all relevant quasiparticles, in two orthogonal directions and an extension in the third, which leads to a coexistence and co-dependence of discrete and continuous properties as seen in electronic, vibrational (phonon), magnetic (magnon), *etc*. spectra that are both dispersive and oscillatory.

The unique features of 1D systems have spurred a wide interest in their fundamentals and led to a variety of applications. The combination of improvements in synthesis and characterisation has resulted in the development of 1D-structure-based devices for optoelectronics, energy, device physics, nanomechanics, biomedicine, and nanochemistry. The full potential of nanowires including a wider context[1-30] is illustrated in Figure 2.2.1 (*cf*. recent reviews 31,32).

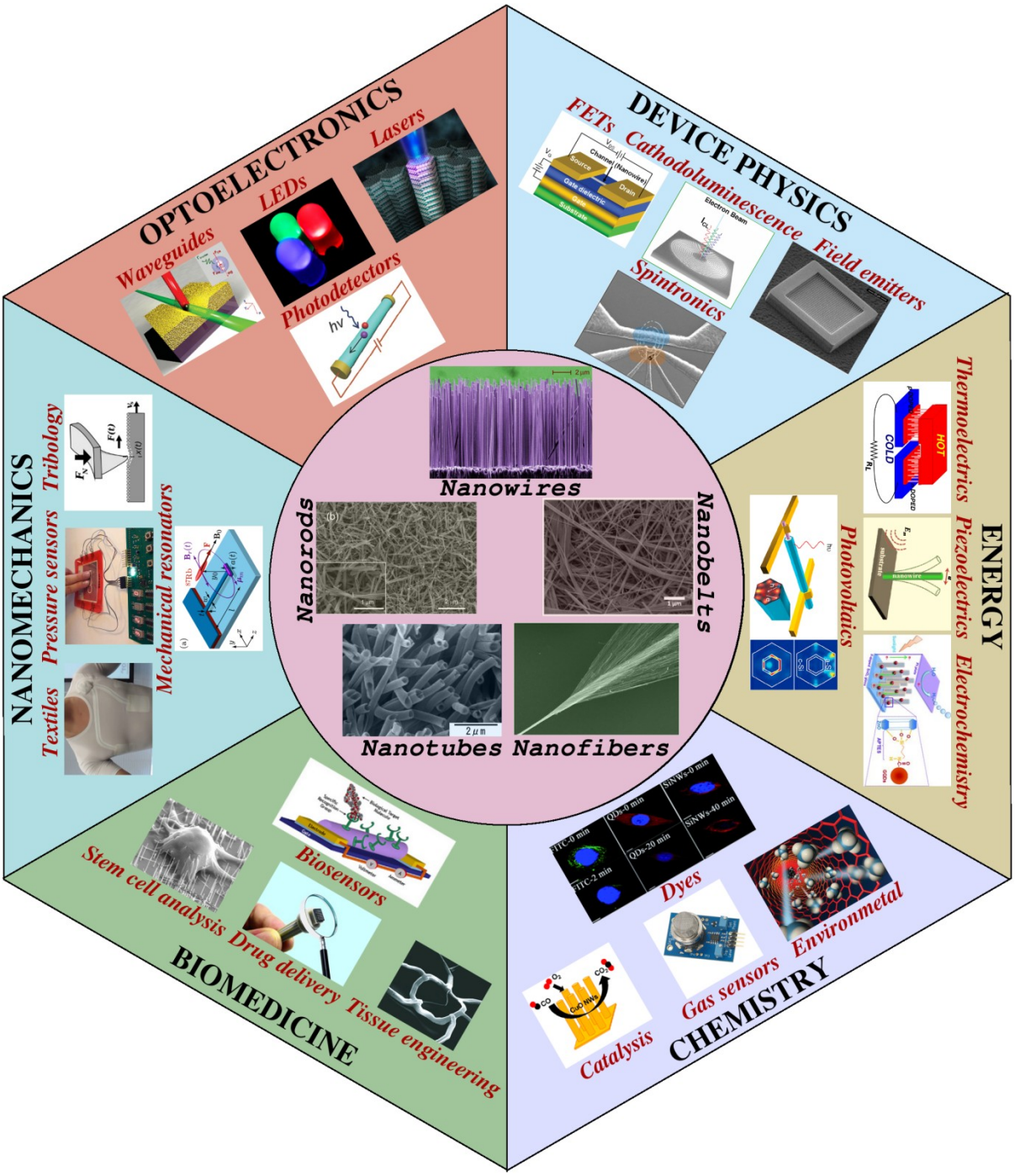

Figure 2.2.1. Applications of 1D materials.

The properties of particular 1D systems are determined by their atomic structure; thicker nanowires behave in many ways like bulk crystallites whereas ultrathin wires and nanorods (segments of nanowire or elongated nanoparticles) have more pronounced discrete features. In direct analogy with hollow cage structures of nanoparticles described in Section 2.1.9 of this book, nanotubes

proved to be readily formed and are well known, especially in their carbon form. The latter has been extensively reviewed, with a number of monographs devoted to them exclusively, *e.g*. references 33-35, and does not warrant further discussion. Different methods of synthesis, preparation and post-synthetic treatment allow complex structures involving the combination of two or more materials, such as nanorods capped or cladded with another material, to be formed, which have numerous advantages.[25] Key to the properties of such systems is how they interact with supports in devices; many nanorods and wires are formed directly on a substrate. An important feature to understand, therefore, in addition to the properties of 1D systems along their extended dimension, is the structure of interfaces. Furthermore, the ability to assemble branch points and tripods using different materials, which are useful for increasing the surface area of adsorber materials and designing nanoscale electrical circuits, involves a combination of interfaces between nanowires, as well as the interface with a substrate or contact. A different form of support is provided by materials with nanoporous architecture capable of hosting 1D nanowires; either singly or assembled in stacking sequences thus giving rise to highly functional nano-composite materials. Typically, materials formed by strongly bound inorganic compounds play the role of the support including zeolites[36] and semiconductors (*e.g.* silicon carbide[37] and zinc oxide[38]), but more recently organic and hybrid metal organic frameworks have found their use.[39,40]

Atomistic and electronic modelling is an essential component in understanding and predicting properties of 1D nanostructures. In this chapter, we will highlight the main contemporary approaches and outstanding examples of their application.

The central challenge to computational approaches in materials science is to bridge the gap between what can be accurately modelled and real life

structures synthesised in the laboratory.[1] The most successful current models have been developed for gas phase molecules on one end of the scale and crystalline materials using three-dimensional (3D) periodic boundary conditions (PBC) on the other. The 1D systems of interest are of course neither; a major model and software development is, therefore, a prerequisite of further work, examples of which are discussed below.

The focus of our research into the structure and properties of 1D systems is localised states, or point defects, the charge of which is perhaps one of the most essential characteristics. An accurate treatment of charged defects, *i.e.* those supporting trapped electrons or holes, is required to model processes of fundamental and applied interest, involving charge transfer and excitations. Another issue is the behaviour of localised states in 1D systems of a large effective diameter, where a large number of atoms (*e.g.* $> 10^3$) must be included in the model. Appropriate methods providing such a treatment for bulk are now routine, but are not applicable to lower dimensional systems.

The rest of this chapter is as follows: the electrostatics of systems extended in one dimensions is discussed first. The essential features of the electronic structure theory in 1D are introduced next. We then discuss the dynamical behaviour, structure, phase stability and transport in 1D. As the next development, kinetic phenomena are overviewed, leading to the studies of defects and wire or tube surface properties.

To illustrate some of the main concepts in this chapter we will use a toy system – an infinite line of atoms with a basis of one or two atoms in a unit cell. The line can either be straight or buckled as shown in Figure 2.2.2, with a

---

1 In this respect the computational science is in a surprisingly good position as the experimentalists report synthesis and preparation of smaller and smaller high quality nanostructures, for which modelling becomes feasible using modern high performance computers.

metallic and covalent character of bonding represented by Si and ionic dielectric behaviour exhibited by ZnO and CdS. Its electronic and vibrational properties will be discussed in detail below.

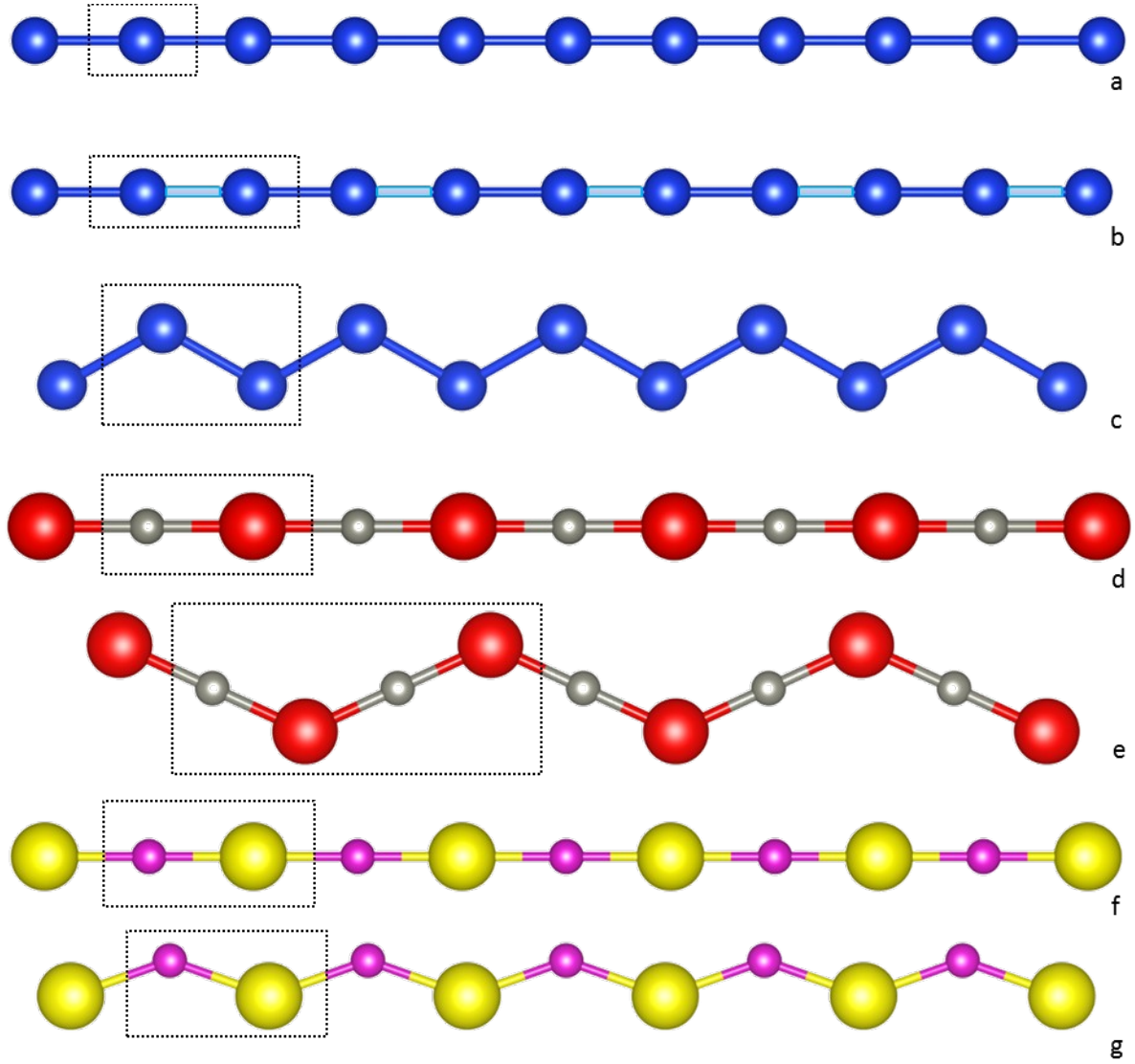

Figure 2.2.2. The infinite 1D Si systems: (a) linear equispaced configuration, (b) dimerised chain, (c) buckled saw-tooth configuration; ZnO (d) linear and (e) buckled chains; and CdS (f) linear and (g) buckled chains. Unit cell is highlighted with a dotted line. Si – blue; Zn –grey; O – red; Cd – violet; and S – yellow.

2.2 Long-term interactions

Energy evaluation, as introduced in the previous Section 2.1, requires an accurate account of many interactions in the system including short- and long-range terms.[2] But in contrast to the finite nanoparticles and clusters, modelling one-dimensional systems encounters one problem, which is common to all extended systems with long-range potentials – the conditional convergence of electrostatic series. “Conditional” does not mean that the convergence is just slow, but that the result of the calculation is mathematically ill defined, which we illustrate below using our toy system of a linear (non-buckled) two-atomic chain with an interatomic distance between nearest neighbours of d (see *e.g.* Figure 2.2.2 (d)). For clarity, in this following analysis we use the atomic system of units. An electrostatic potential on atom A with a negative charge q can be calculated as a series of contributions from more and more distant pairs of atoms symmetrically arranged around A, whose charge alternates between $+q$ and $-q$,

$$\varphi = \frac{2q}{d}\sum_{n=1}^{\infty}\frac{(-1)^{n+1}}{n}. \qquad (2.2.1)$$

The astute reader will have noticed that this infinite sum is a particular case of the Taylor expansion of $\ln(1+x)$ around zero with $x=1$:

$$\ln 2 = \sum_{n=1}^{\infty}\frac{(-1)^{n+1}}{n}. \qquad (2.2.2)$$

Let us have a careful look at this series:

$$\sum_{n=1}^{\infty}\frac{(-1)^{n+1}}{n} = 1-\frac{1}{2}+\frac{1}{3}-\frac{1}{4}+\frac{1}{5}-\frac{1}{6}\cdots \qquad (2.2.3)$$

We can rearrange its terms, for example thus,

---

2 Note, however, that some atomistic models, in particular for covalent and metallic systems, neglect completely the long-range interactions, *e.g*. using bonding harmonic or embedded atom force fields, respectively.

$$\left(1-\frac{1}{2}\right)-\frac{1}{4}+\left(\frac{1}{3}-\frac{1}{6}\right)-\frac{1}{8}+\left(\frac{1}{5}-\frac{1}{10}\right)-\frac{1}{12}+\left(\frac{1}{7}-\frac{1}{14}\right)\cdots=\frac{1}{2}-\frac{1}{4}+\frac{1}{6}-\frac{1}{8}+\frac{1}{10}-\frac{1}{12}+ \quad (2.2.4)$$

which demonstrates that convergence of the series is conditional. The physical implication of this behaviour is that the total energy of a 1D system is not defined, neither is any related property such as the work required to remove or add a charged particle to the system in a particular location, *i.e.* to create a point defect.

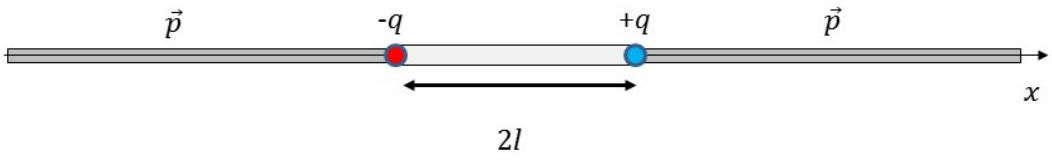

Figure 2.2.3. A model of an infinite 1D chain of dipoles with density *p*.

The origin of this unphysical result is usually related to an uncertainty introduced by assumption that the 1D system is infinite in length. If, instead of an infinite chain, we considered its finite neutral fragment (a rod) of length 2*l*, then charges $\pm q$ that terminate the chain on both ends would define the overall rod dipole $\vec{P}$ and therefore its potential at any point sufficiently removed from the rod (*i.e.* where the atomic structure can be neglected). So we can associate with the system a dipolar density $\vec{p}=\vec{P}/2l=q\vec{e}$ (see Figure 2.2.3). By applying the cyclic boundary conditions to the system, we would recreate the original infinite chain, with a dipolar density, or polarisation, $\vec{p}$, the value of which depends on the termination procedure. This arbitrary choice gives rise to an uncertainty in the potential reference in 1D, but in contrast to 3D bulk systems the electric field is defined uniquely as the corresponding series converges absolutely.

In nature (or the laboratory), any such system is of course finite and terminated in a particular fashion, setting the values of both potential and field uniquely. If the “macroscopic” local field is nonzero, the system would be ferroelectric and would naturally acquire a domain structure, where the voltage the charge carrier is subjected to should be commensurate with usual physical constraints, for example that of a characteristic band gap discussed in the next section. More often however, the field will be very close to zero (subject only to local fluctuations), and the potential will be uniquely determined by ordering terms in the electrostatic series such that each fractional sum corresponds to a fragment with a zero dipole. With the value of the potential thus defined, there is still however a problem due to the slow convergence of the series.

To tackle this problem of slow convergence, in an ingenious and very popular Ewald’s approach,[41] a Coulomb potential is split into two contributions: one short and another long range. The short range term is summed up directly over the lattice where the speed of convergence can be tuned with a careful choice of the potential form and parameters, customarily defined as the Coulomb potential of a Gaussian charge distribution. The long-range term can be easily evaluated in reciprocal space, where its Fourier transform is short-ranged and the therefore the corresponding sum converges quickly. Mathematical details of this technique and its application to systems of different dimensionalities can be found, for example in references [42] and [43]. Notably, an alternative approach implemented in a number of atomistic and electronic structure codes has been proposed by Saunders et al.[44], who exploited the Euler-MacLaurin summation formula rather than Fourier based constructs.

Finally, we note that only few current codes tackle specifically 1D boundary conditions; however there are many *ab initio* and atomistic (in particular, molecular dynamics, or MD) codes providing accurate treatment of

any systems in 3D. Therefore a popular choice for modelling lower dimensional systems is a supercell approach, in which for example a wire is modelled within one unit cell surrounded in two directions by a layer of vacuum. Periodic repetition of this unit cell in all three dimensions results in an infinite stack of nanowires arranged on a 2D lattice. Although this system could be of interest as it reflects the real situation of nanowire synthesis in some cases, more often the resulting interactions between periodically repeated nanowires is completely fictitious. To improve the model, one should remove these interactions, which can be incorporated in the relevant code or done *a posteriori*, which is an area of continuing development, see e.g. reference [45].

2.3 Energy and electronic structure theory

Having established the electric potential, in the field of which move all charge carriers, we now discuss the energy states of such charge carriers. We begin by briefly recalling qualitative theories of the electronic structure of 1D periodic systems. This approach is commonly used in solid state texts as an introduction to band theories of crystalline solids, but as we concern ourselves with 1D rather than 3D, we feel that such a recall is beneficial for the reader.

In a 1D system characterised by a linear coordinate x, an electron in a stationary state is described by a wave function, $\psi(x)$, which is subject to the corresponding Schrödinger equation with an external general potential, $\hat{V}(x)$:

$$\hat{T}\psi(x)+\hat{V}(x)\psi(x)=E\psi(x), \tag{2.2.5}$$

where $\hat{T}=\frac{-\hbar^2}{2m_e}\nabla^2$ is the kinetic energy operator, $\hbar$ the reduced Planck's constant, m_e the electron mass, and E the electron energy. For simplicity, we will assume here that the potential is local, working as an operator of multiplication by a function of argument x, with a hat dropped. We now introduce periodic boundary conditions so that

$$V(x+L)=V(x), \tag{2.2.6}$$

with L being the period of potential (the unit cell parameter in 1D). Bloch's theorem states that solutions to eq. (1) should take the form:

$$\psi_{nq}(x)=e^{iqx}u_{nq}(x), \tag{2.2.7}$$

where $u_{nq}(x)$ is a periodic function with the same periodicity as V. The two indices number possible solutions of eq. (2.2.5). One simple implication is:

$$\psi_{nq}(x+L)=e^{iq(x+L)}u_{nq}(x), \tag{2.2.8}$$

Then for ψ to be a solution of eq. (1),

$$\psi_{nq}(x+L)=e^{iqL}\psi_{nq}(x). \tag{2.2.9}$$

The two indices numbering wave functions have their correspondence in the electronic energies, which form the band structure. The index q is not unique as

$$q, q\pm\frac{2\pi}{L}, q\pm 2\frac{2\pi}{L}\ldots \tag{2.2.10}$$

give identical wave functions and energies. To describe the complete band structure it is therefore sufficient to consider only the range of $q[-\pi/L, \pi/L]$, known as the reduced zone scheme.

In fact, spectra of elementary excitations of quasiparticles in extended systems are described with wave like equations closely related in their form to eq. (2.2.5) and therefore have similarly structured solutions. An important example, considered in Section 2.2.4, is the case of phonons, which are quantised waves of atomic vibrations.

Further, for a given value of q, there is an infinite number of solutions, which we typically index with n from low energy to high. The lowest energy solutions correspond to the bound electronic states of atoms or molecules, from which the unit cell (*i.e.* the smallest repeatable unit in the periodic system) is made up; they are occupied by the core and valence electrons and can be separated from or merge with the higher lying extended states. For an atom, the full electronic energy spectrum consists of two parts – lower-energy discrete and higher-energy continuous; for the periodic system, because of the variation of energy with q, both parts of the spectrum are continuous. However, the discrete nature of the bound states is retained in the spectra of the periodic system in the form of discrete bands (which may, however, overlap with each other) as will be seen below.

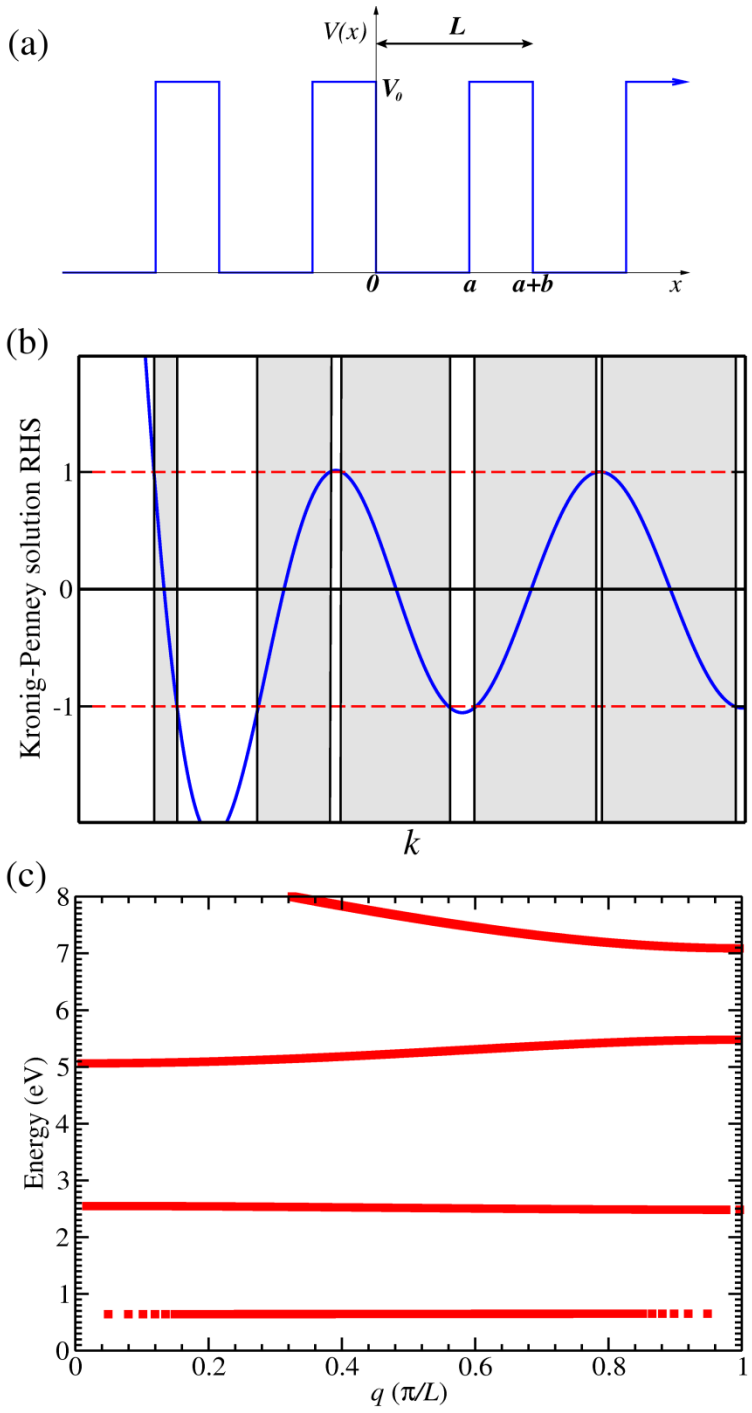

Figure 2.2.4. Kronig-Penney model: (a) potential, (b) solution, and (c) dispersion.

The origin of the discrete bands can best be described in terms of the simplest example of an electron confined within a 1D system, *i.e.* the Kronig-Penney model, which consists of a periodic array of potential wells, each of width a, separated by barriers of width b and height V_0, as shown in Figure

2.2.4(a). Given Bloch's theorem (Eq.(2.2.8)), the allowed solutions of Schrödinger's equation for an electron with energy E subject to such a potential are linear combinations of plane waves, the wavenumbers q of which are constrained by the boundary conditions:

$$\cos q(a+b)=\cos ka\cosh \kappa b+½(\kappa/k-k/\kappa)\sin ka\sinh \kappa b, \quad (2.2.11)$$

where $k=\sqrt{2m_e E}/\hbar$ and $\kappa=\sqrt{2m_e(V_0-E)}/\hbar$. If we plot the right-hand side (RHS) of Eq. (2.2.11) as a function of k (see Figure 2.2.4(b)), it is immediately obvious that, for certain values of k (or equivalently E), its magnitude is greater than 1, which is incompatible with the left-hand side, indicating that the equation at this value has no solution. Such values of k or E make continuous bands of forbidden states and are commonly referred to as energy gaps. When we consider q as a function of E, *i.e.* the band structure, we observe alternating intervals of allowed and disallowed states, with one example (with a=6 Å, b=4 Å and V_0=6 eV) given in Figure 2.2.4(c). The range of q is confined within the reduced zone scheme, which is the 1D first Brillouin zone. The band structure can be used to derive other important features such as the electron (or hole) effective mass m^*, and the density of states (DOS), which shows band widths and gap values, on which many optical and transport properties depend.

A realistic potential in eq. (2.2.5), however, will be much more complicated, reflecting the chemical nature of the system, and, unfortunately, there are no simple closed solutions to (2.2.5). To simplify the problem, a basis set is introduced, which can either refer to the behaviour of the electron bound to a nucleus, as in an atom, or to the extended plane-wave like nature of a nearly free electron. The former approach is employed by tight binding, or model Hamiltonian methods, whereas the latter by model potential techniques. Such methods typically rely on empirical parameters fitted to reproduce experiment or, more recently, high-level *ab initio* calculations. A modern implementation of model potentials, in particular in the field of quantum chemistry of molecules on one hand and solid state physics the other, takes the form of semi-local pseudopotentials, which account for the core electrons – see for example references [46-50]. One can then separate the many-electron system into core and valence electrons, treating the valence electrons explicitly, which move in the field of not just nuclei but also core electrons.

The band structure discussed so far relates to states that extend along the periodic spatial dimension of the 1D system. In the other two orthogonal directions quantum confinement will determine the form of the electronic states. The degree to which confinement has an effect depends on the thickness of the nanowire, where the typical localisation length of the corresponding state should be compared with the characteristic confining dimension.

The one-electron picture discussed so far is in many respects too simplistic, when we consider real systems of many electrons, and a number of more appropriate accurate theoretical approaches of various sophistication have been developed and implemented in commonly accessible software packages. The essential features of the electronic band structure, which we highlighted using a simple Kronig-Penney model, are retained for the majority of systems of interest.

Key exceptions concern systems with critical two- or more electron behaviour observed, for example, in the superconducting regime. As the electronic system in quantum mechanics is described by a many-electron wave function, the solution of a many-electron analogue of eq. (2.2.5) becomes necessary but intractable. The applied studies typically employ one of the following levels of theory, which accounts for the quantum-mechanical many-electron interactions, that is exchange and correlation:

1. Mean field and Hartree-Fock theory. The simplest approach to treating electron-electron interactions is to model each electron in the mean field due to all electrons in the system, or rather their charge density. The obvious fault with such an approach is an ensuing self-interaction of an electron which, perhaps, could be insignificant for systems in which there are very large numbers of electrons. Importantly, however, in close proximity to a given electron at a given position and time, we should expect depletion in the probability to find other electrons, due to both Coulomb repulsion and the Pauli Exclusion Principle. The former dynamical effect (and other related phenomena involving interactions with more than two electrons) is referred to as electron correlation and the latter, which concerns only same-spin particles, electron exchange. Mean field theory, although neglecting these interactions, only requires the solution of the one-electron Schrödinger equation ((2.2.5))) in an external local potential derived from the total charge density (known as the Hartree potential). By introducing an anti-symmetric many electron wave function, in an approach known as Hartree-Fock theory, one can derive a potential that contains a local (Hartree) term, and a non-local (Exchange) term, so that electron exchange is treated explicitly. The formulation of these terms leads to a fortuitous cancellation of the self-interaction energy. The

drawback, however, is an increased complexity in the calculation due to the non-local term. Thus, to describe *n* electrons we need *n* one-electron orbitals, a problem which becomes tractable using modern computers.

2. Semiempirical methods that originate from the Hartree-Fock theory using a minimal basis of localised atomic valence orbitals, where the matrix elements associated with three or more atomic centres are omitted and one- and two-centre terms are approximated using simple analytical functions, which are then parameterised and fitted to experimental and/or *ab initio* data. The variability in the chemical environment is treated by these methods via an SCF (self-consistent field) procedure in full analogy with the parent *ab initio* approaches. SCF versions of tight binding approaches have also been developed and widely applied to the study of nanosized systems.
3. Density Functional Theory (DFT), where the total energy of the system is represented as a functional of the charge density. The pragmatic approach in the Kohn-Sham formulation of DFT is, in analogy with the mean field approach, to map the many-electron function to a single-particle orbital, representing an idealised electron moving in the mean field of all electrons (including itself) and nuclear (core) charges, now also including exchange and correlation effects. Although in principle exact, the potential (exchange and correlation) contribution from all the electrons is not generally known, and therefore requires some form of an approximation. The simplest Local Density Approximation (LDA) assumes a full locality of the potential that only depends on the charge density at the point, where it is probed, and is usually equated with the known potential of a homogeneous electron gas of the given density. Further more sophisticated approximations include the first derivatives of the charge density (Generalised Gradient Approximation, GGA), the second

derivatives of the charge density and/or kinetic density (Meta-GGA), and a fraction of exact Hartree-Fock exchange (hybrid-DFT). In all of these methods occupied Kohn-Sham orbitals are used to construct the potential and energy.[51] Recently, even more sophisticated methods using unoccupied Kohn-Sham states have been advanced, termed double hybrids.[52]

4. Many-electron theories, in contrast to DFT, include an explicit account of electron-electron interactions. In the first instance, the total energy can be constructed as a series of consecutive improvements over the Hartree-Fock approximation, taking into account correlation between pairs, trios, and higher order combinations of particles in a perturbative or “exact” manner, leading to Møller-Plesset (MP*n*) and coupled cluster (CC) methods on one hand, and configurational interaction (CI) and multiconfigurational (MC) SCF techniques on another. An analogous, closely related family of methods deals with the problem of one-, two- and more particle spectral properties of the system by employing the formalism of Green’s functions, which is also used for the treatment of localised defect states and transport. The most widely used approaches include: GW, as applied to calculations of ionisation and attachment energies, thus allowing direct comparison with experimental photo- and secondary electron spectra; the Random Phase Approximation (RPA), typically used in the same context as GW, but recently applied with significant success to calculating the total energy when perturbative single and double excitations are treated (both GW and RPA are also used for the calculation of the dielectric function); and, finally, the Bethe-Salpeter (BS) equation, which describes explicitly two-particle interactions within a many-particle system and allows accurate modelling of excitonic spectra. All these approaches are very

expensive with respect to computer resources, but are becoming more accessible as the years pass by.

To highlight the main features of 1D band structures and DOS, we have calculated the band dispersion for a series of toy linear chain systems (see Figure 2.2.2) using hybrid DFT. The chains are assumed to repeat periodically in the *x* direction, with a unit cell length of *a*. For each system, we have either carried out full geometry optimisation or, in the case of perfectly linear chains, optimised the structure with symmetry constraints. All calculations have been performed using the VASP code,[53-56] with the projector augmented wave (PAW) approach[57] to describe the interaction between the core (Si:[Ne], Cd:[Kr], Zn:[Ar], S:[Ne], O:[He]) and valence electrons, and the solids-corrected Perdew-Burke-Ernzerhof GGA exchange-correlation density functional with 25% exact Hartree-Fock exchange included (PBEsol0).[58-61] Total energy convergence within 10^{-4} eV/atom has been achieved using a plane-wave cut-off energy of 1200 eV and a $48 \times 1 \times 1$, $24 \times 1 \times 1$, $12 \times 1 \times 1$ Monkhorst-Pack *k*-point mesh for the one, two, and four atom unit cell cases, respectively. Calculations were deemed to be converged when the forces on all atoms were less than 0.01 eV $Å^{-1}$.

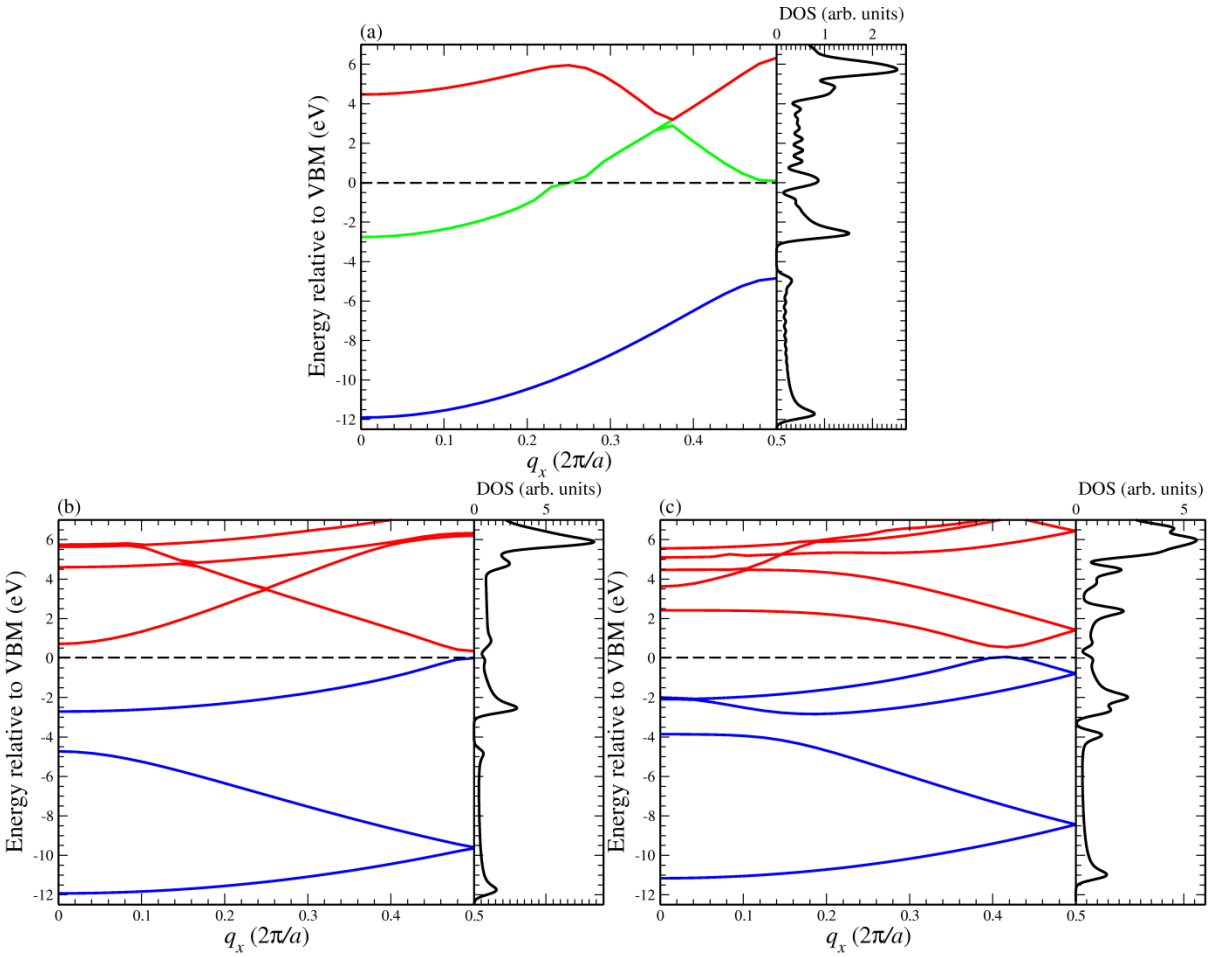

Figure 2.2.5. Band structure and density of states of the (a) linear, (b) dimerised, and (c) buckled Si chain. Here and below, blue lines are used for valence states (bands), red for conduction.

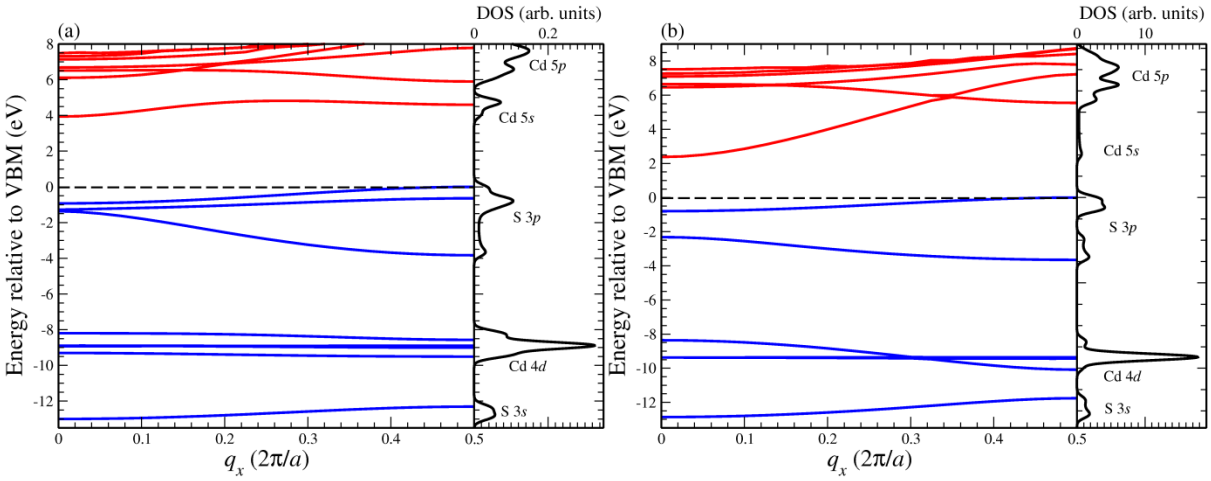

Figure 2.2.6. Band structure and density of states of the (a) buckled and (b) linear CdS chain.

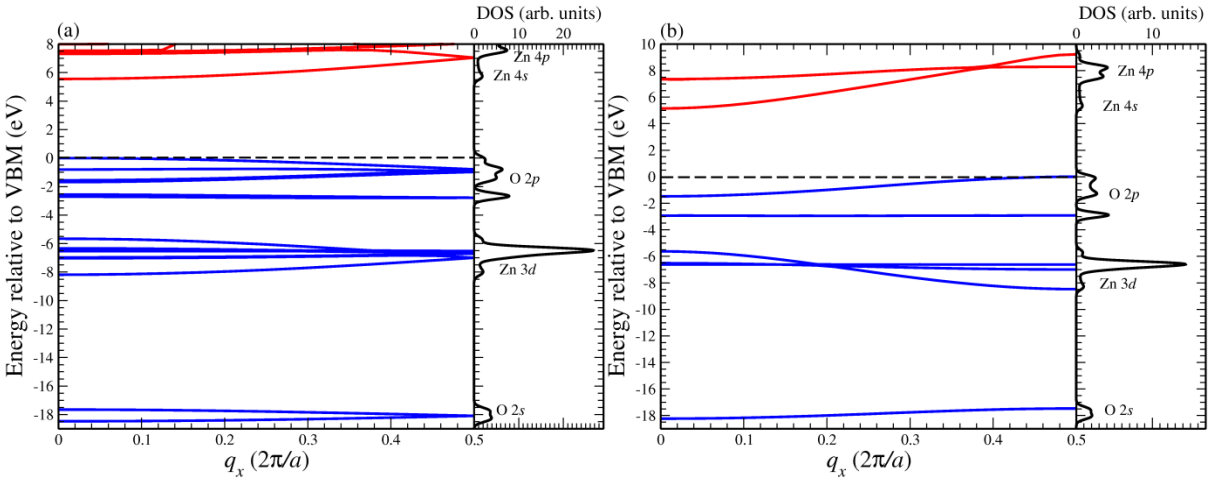

Figure 2.2.7. Band structure and density of states of the (a) buckled and (b) linear ZnO chain.

The calculated band structures and DOS are shown in Figures 2.2.5-7. In all cases we observe cosine-like dispersion, as expected from our discussion on the Kronig-Penney potential above. For the ionic bonding cases, we have indicated the orbital contributions to the DOS, which demonstrates the origin of the bands. We now discuss the particular cases in more detail.

For metallic and covalent bonding, we have chosen Si as a representative system. The perfectly linear case, Figure 2.2.2 (a), consists of a single Si atom in the unit cell, with a Si-Si bond length of 2.12 Å. This structure is unstable with respect to a Peierl's type distortion (see Section 2.2.5 below), which can be traced to its unpaired electrons occupying orbitals perpendicular to the chain. The system is metallic, as can be seen from the band structure, Figure 2.2.4 (a), where the metallic band is shown in green. Two distortions can occur to break the symmetry and lead to electron pairing: dimerisation (Figure 2.2.2 (b)) and buckling (Figure 2.2.2 (c)). In both cases, the unit cell doubles to two atoms per cell. We find that buckling, where the Si-Si bond length increases to 2.20 Å and the bonds form an angle of 117.11°, is the ground state, being 0.56 eV/atom more stable than the linear case (and 0.52 eV/atom more stable than the dimerised case). Looking at the band structures (Figure 2.2.5 (b) and (c)), we

observe band folding due to the increased unit cell sizes, and clearly see a direct band gap opened up (0.46 eV for the dimerised chain, 0.49 eV for the buckled chain). The reduced symmetry of the buckled chain is reflected in the breaking of degeneracy of the bands.

For ionic bonding, we have considered two systems: CdS and ZnO. The main features we observe in the band structures (Figures 2.2.6 and 7) are a large band gap (approx. 2 and 5 eV) between anion *p* (making up the top of the valence band) and cation *s* orbitals (making up the bottom of the conduction band), and localised (low dispersion) orbitals deep in the valence bands (cation *d* and anion *s* orbitals). For CdS, the buckled chain structure (Figure 2.2.2 (g)), with two atoms in its unit cell, is 0.18 eV/atom more stable than the linear chain (Figure 2.2.2 (f)). Due to the buckling (with an angle of 140.56°), the Cd-S bond length shortens from 2.37 to 2.29 Å, which results in a greater anion-cation repulsion and a corresponding increase in the band gap (from 2.38 to 2.93 eV). On buckling, the breaking of degeneracy within the *p* and *d* orbitals is evident from the band structures.

For ZnO, a similar set of results to that of CdS was found, apart from one important difference: the buckling of the chain occurred so that the Zn ions remained linearly coordinated. This coordination means that the unit cell consists of four atoms (see Figure 2.2.2 (e)), which leads to a folding of the bands due to the reduced reciprocal unit cell size. The buckling angle is 130.31°, and the Zn-O bond length reduces from 1.742 Å to 1.736 Å, with a resulting increase in band gap from 5.15 eV to 5.55 eV.

A large number of studies have been performed to determine the band structure of various nanowire systems, a representative set of which we list next. Si nanowires are the most well studied, using computational approaches including k•p,[62] tight-binding,[63] and DFT.[64-66] A comprehensive k•p study of core-

shell nanowires for III-V systems has been performed by Pistol,[67] including Γ-point energies and effective masses, while the band structure of InAs nanowires has been determined using a tight-binding approach by Lind.[68] Ballistic transport through the 1D subbands is included in many of these studies. In all cases the calculated band structures display the basic features of those of our toy models, as is evident for example from a DFT study on Si nanowires by Nolan et al.[65] – see Figure 2.2.8. Experimental techniques used to study electronic bands in 1D nanosystems include resonant Raman spectroscopy (comparing the electronic structure of GaAs in wurtzite and zinc blende phases),[69] angle-resolved photoluminescence spectroscopy,[70] photoluminescence (PL),[71] time-dependent PL and PL excitation,[72] and conductance measurements.[73]

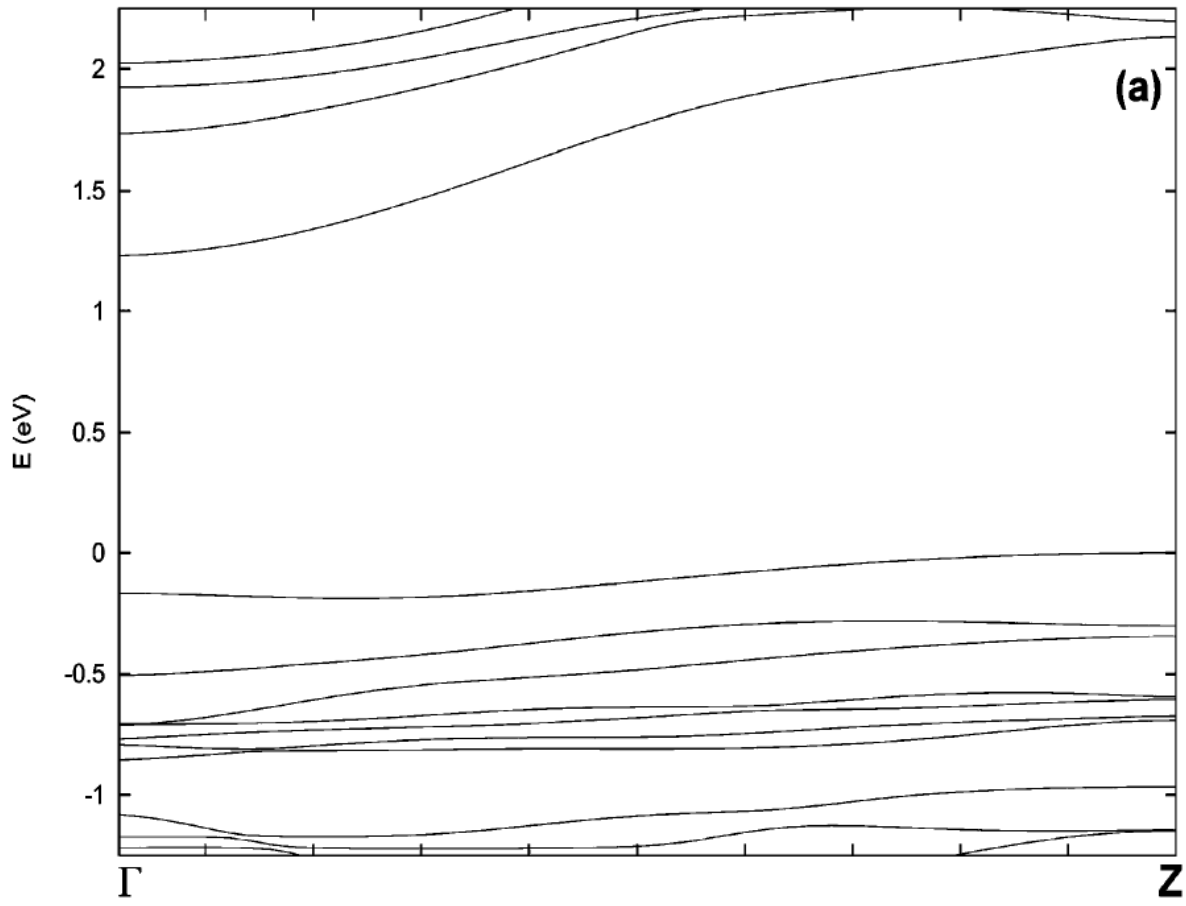

Figure 2.2.8. Calculated band structure of Si nanowires using DFT.[65]

2.4 Dynamical properties

The structure and properties of 1D systems in equilibrium are still of course affected by the thermal motion of atoms and, in particular, at low temperatures, by its quantum character, which should be expected based on the uncertainty principle. The fact that we are able to describe the electronic properties without recourse to the nuclear motion is a consequence of the dramatic difference in particle masses between an electron and even the lightest nucleus, *i.e.* a proton. Such a separation of the electronic motion from the nuclear is described by the Born-Oppenheimer theory, which uses the ratio of these two masses as a small parameter $\sim O(10^{-3})$, about which the total energy of an electron-nuclear system is expanded. As the electronic energy can be determined for a given set of nuclear coordinates, it may be considered as a potential, in the field of which nuclei move, which forms the basis of the semiclassical method of interatomic potentials – see the preceding chapter.

The potential energy of any system is a smooth function of nuclear coordinates, about which it can be expanded into a Taylor series. Typically, the potential energy of nuclei (usually referred to as atoms in this context) is sufficiently well represented by harmonic wells with a possible inclusion of anharmonic corrections, which corresponds to retaining the quadratic and higher-order cubic terms (the first order term drops out as a necessary condition of the system stability). On average, the atoms can be found at the bottom of these wells, and the first computational task in a study of a material is to determine positions of these minima, the object of geometry optimisation discussed in full in Section 2.1.

When the coordinates of the minimum of interest are found, the thermal motion around the minimum can be described classically, in the harmonic approximation, as a system of coupled linear oscillators. The solution of the

problem leads to a set of eigenmodes, within which the atomic system can vibrate. The corresponding quantum-mechanical description involves the quantisation of such modes into particles of atomic vibration known as phonons. By pumping in the energy into a particular eigenmode, at a classical level, we increase an amplitude of the corresponding atomic oscillation, or, at a quantum-mechanical level, we generate more phonons of a particular eigenenergy (or frequency). The eigenmodes are in practice vectors of pre-exponential coefficients in a plane-wave representation of waves propagating through the system, which are subject to the same periodic boundary conditions considered above for electrons and consequently an analogous Bloch theorem. For each atom in a unit cell there are three spatial degrees of freedom, so there are three corresponding unique phonon (vibrational) modes, implying a very large number for an extended system, which can however be conveniently enumerated using **q**-points in the reciprocal space, all within just one, 1st Brillouin zone. If our unit cell contains M atoms, the number of possible modes due to just these atoms will be $3M$, which is the number of branches spanning the 1st Brillouin zone, with the energy (frequency) dependence on the **q**-point known as dispersion. The three lowest frequency modes are termed the acoustic modes, as in the elastic limit they correspond to sound waves in the solid, and consist of in-phase motion of the atoms within the unit cell. Any other modes are termed optical, and consist of motion where the centre of mass of the atoms remains constant, implying a well-defined phase difference between their individual vibrations.

Similar to electrons, in 1D, the atomic degrees of freedom may be restricted, depending on the level of confinement. In the two orthogonal directions where periodicity is removed, the phonon modes become restricted or confined, which alters their dispersion. This lack of periodicity results in much larger unit cells, which in turn leads to an increase in the number of eigenmodes.

Moreover, surface scattering leads to a lifetime or broadening of the modes which can be directly observed using Raman spectroscopic techniques. In order to demonstrate the basic concepts of phonon dispersion in 1D systems, we now discuss the dynamical properties of our toy 1D chain systems presented in Figure 2.2.2.

Phonon frequencies have been calculated with a frozen phonon approach, which requires knowledge of second derivatives of energy (force constants) with respect to atomic degrees of freedom in a suitably chosen supercell (24 atom unit cells in all cases discussed below). The force constants were evaluated numerically, employing the method of finite atomic displacements and energy and forces calculated at the hybrid DFT level (introduced in our discussion of the electronic bands in Section 2.2.2). q-point interpolation as implemented in the post-processing program PHONOPY[74] was then used to determine the dynamical matrices and phonon dispersions.

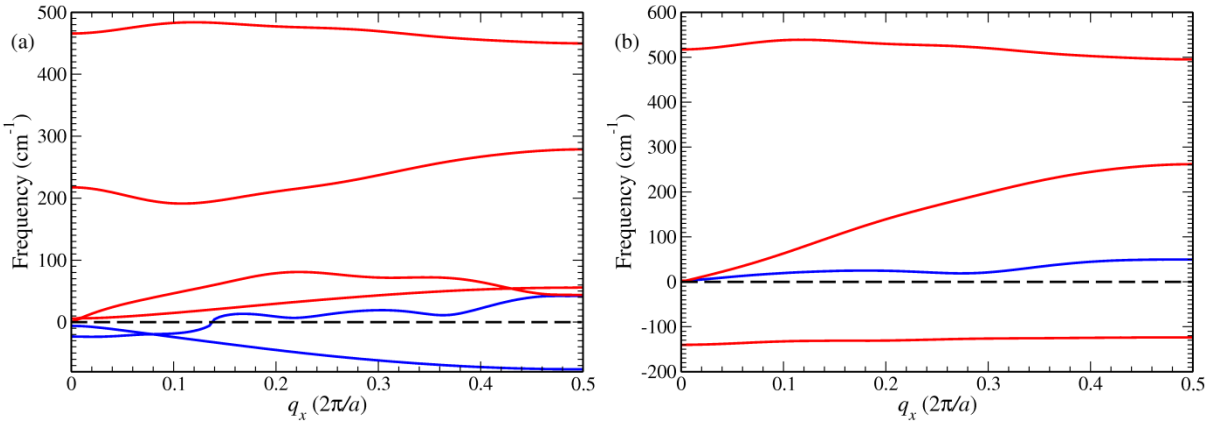

Figure 2.2.9. Phonon dispersion of the (a) buckled and (b) linear CdS chain.

We first discuss the ionic system CdS (Figure 2.2.9). In Section 2.2.2, we found that the buckled chain was lower in energy than the linear chain. For both the linear and buckled chains, as we have two atoms in the unit cell, there are six phonon modes, three acoustic and three optical. The transverse acoustic (TA) modes (shown in blue in the figures) consist of perpendicular displacements of the chain, and remain at low frequencies throughout the Brillouin zone (BZ). The

longitudinal acoustic (LA) mode has linear dispersion close to the Γ point, the slope of which is the speed of sound (as in bulk). For the linear chain, the transverse optical (TO) modes are imaginary, indicating that the system is unstable with reference to a distortion along these modes. As these modes consist of out-of-phase motion of the two atoms in the unit cell perpendicular to the chain, this distortion corresponds to the buckling of the chain, *i.e.* a phase transition to the lower energy buckled configuration. The TA modes in this case are degenerate, as expected for a linear chain. The longitudinal optical (LO) mode remains relatively dispersionless at approximately 500cm^{-1}. For the ground state buckled system (Figure 2.2.9 (a)), the dispersion becomes more complicated. The TA and TO modes are no longer degenerate, and the TO mode corresponding to a 'wagging' motion of the ions softens to lower frequency (ranging from just above 0 cm^{-1} to 56 cm^{-1} over the BZ). The LO mode also softens slightly. It is worth noting that the calculated Γ point frequencies of the optical modes (218 and 466 cm^{-1}) are in reasonable agreement with Raman measurements on CdS nanowires (301 and 598 cm^{-1}),[75] when one takes into account the red shift due to confinement, as our system is the limiting case of one atom thick wires. One of the TA modes, however, in this case becomes imaginary, which indicates that the system is unstable. We show how this instability is resolved in the following example of the ZnO chain.

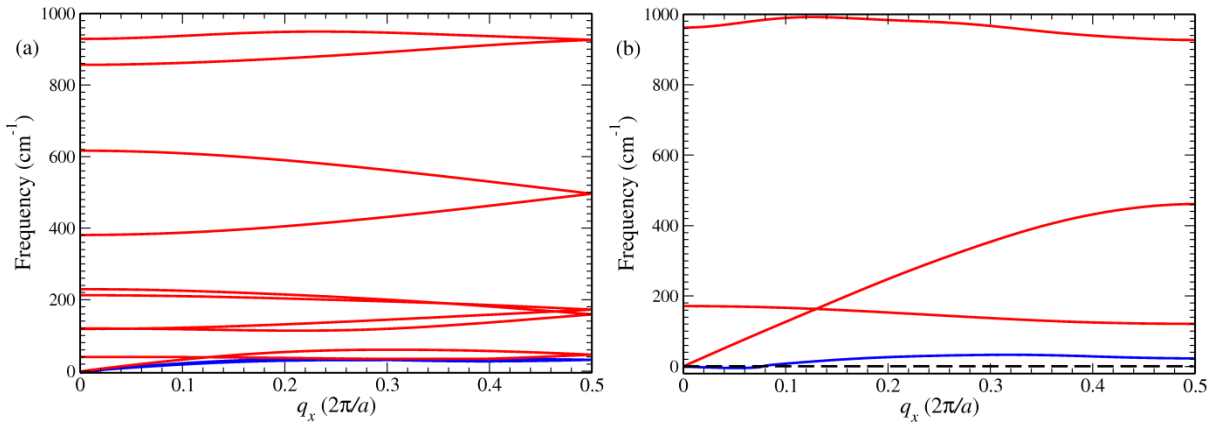

Figure 2.2.10. Phonon dispersion of the (a) buckled and (b) linear ZnO chain.

The results for the ZnO chain display common features to those of CdS, apart from some important distinctions. We remind the reader that the ground state for this system is the buckled chain (Figure 2.2.2 d) with a four atom unit cell. For the linear chain (Figure 2.2.2.b), the modes observed are similar to those of the linear CdS chain, except for an increase in frequency of the LO and LA modes, reflecting the stronger Zn-O interaction, real TO modes (that range from ~170 to 120 cm^{-1} across the BZ), and lower frequency TA modes. The TA modes remain close to zero up to q_x=0.6 (2pi/a), which may be an artefact of the calculation (these modes are low frequency sound waves, and it is possible that their low frequency is within the numerical error of our simulation). The fact that all modes are real indicates that the linear chain is stable, in contrast to the CdS case. The lower energy structure, i.e. the four-atom unit cell buckled chain, is therefore arrived at by a first order phase transition, in which an energetic barrier must be overcome. We will discuss phase transitions in more detail in Section 2.2.5 For the buckled chain (Figure 2.2.10 (a)), we see folding of the phonon bands due to the increased unit cell size, resulting in a doubling in the number of bands, and a splitting of the transverse modes.

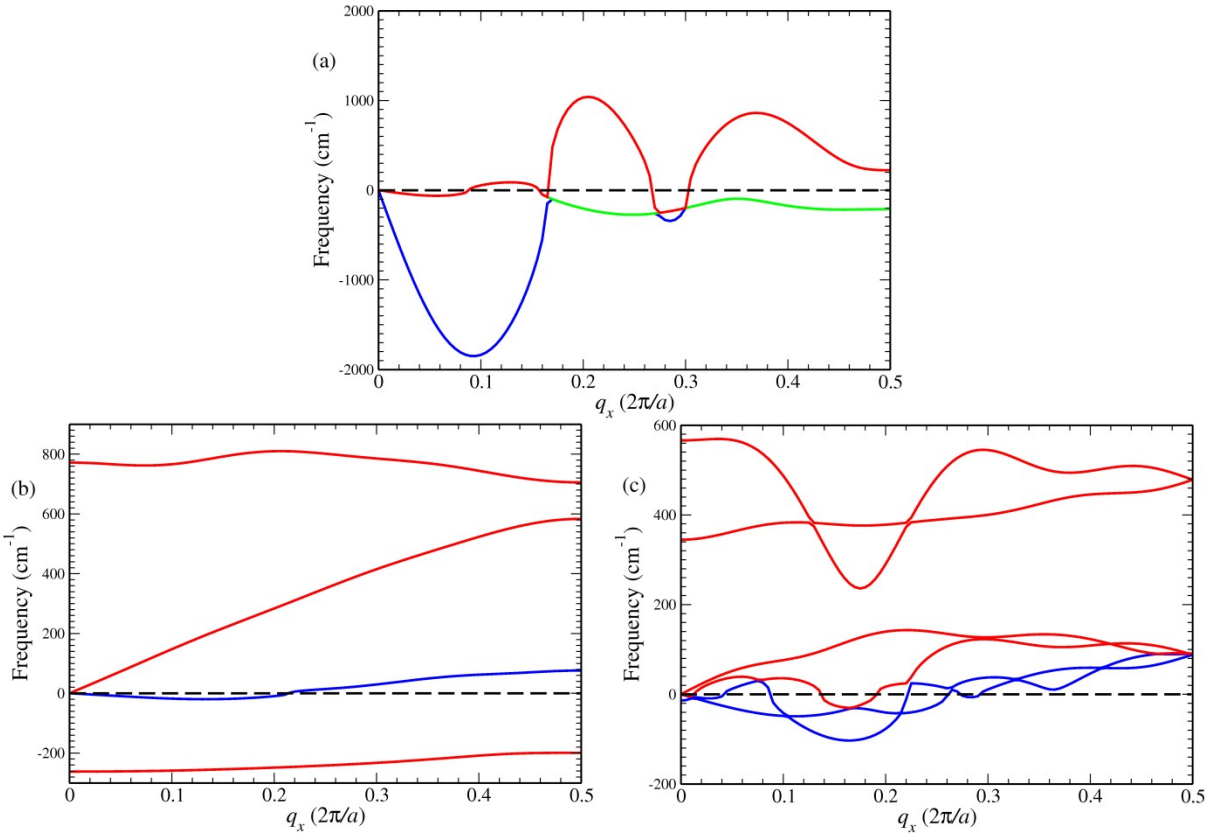

Figure 2.2.11. Phonon dispersion of the (a) linear, (b) dimerised, and (c) buckled Si chain.

The case of the Si chain is somewhat more complicated. The linear chain is unstable with respect to a Peierl's distortion (see Section 2.2.5), meaning it can dimerise (Figure 2.2.2 (b)), but the ground state consists of a buckled chain (Figure 2.2.2 (c)). The instability of the linear chain is reflected in its phonon dispersion (Figure 2.2.11 (a)). As the unit cell consists of a single Si atom, there are only three modes, all of which are acoustic. The LA mode becomes imaginary away from the Γ point, corresponding to the dimerising distortion. The TA mode at the edge of the BZ (shown in green) is also imaginary and corresponds to a buckling distortion. For the dimerised case (Figure 2.2.11 (b)), the dispersion is similar to that of the CdS linear chain, as one would expect (as both are linear and unstable). In this case, there are optical modes, as the unit cell consists of two atoms. The (degenerate) TO modes are imaginary, reflecting the fact that the buckling distortion is energetically preferred by the system. For the buckled

chain (Figure 2.2.11 (c)), the TO modes are no longer imaginary, but one of them (the 'wagging' mode) becomes mixed in with the TA modes. The oscillations visible in these modes' dispersion is a result of the insufficiently large size of supercell we could afford using modern supercomputers. The higher-frequency LO and TO modes are well separated at Γ, but mix as q_x varies across the BZ. Interestingly, at the zone boundary the modes become degenerate, reflecting the fact that the unit cell consists of one species, meaning that the mode distortions in different directions become equivalent when the phase between the unit cells is exactly opposite (which is the case at the zone boundary).

The effect of quantum confinement on the phonon modes in 1D systems has been extensively studied in the literature, from which we provide some examples. Using Raman spectroscopy, the resulting shift and broadening of the optical modes due to confinement have been observed for example in nanowires of Si,[76-78] GaAs,[79,80] CdS,[75] SiC,[81] and GaN.[82] Other experimental techniques have also been used to study the confinement of phonon modes, including optical absorption in CdTe nanowires[83] and inelastic transitions between nanostructures as a probe in InAs nanowires.[84] Such modes were used to explain the low thermal conductivity, and conversely high Seebeck coefficient of Si nanowires,[85,86] by illustrating that confinement leads to surface scattering of optical modes, but efficient transmission of acoustic modes due to the wire diameter being less than the wave length of the phonon mode.

Theoretical studies on the dynamical properties of 1D systems have also been reported. The confinement-induced shift and broadening of optical modes were shown to be strongly affected by the surface structure by Richter *et al*.[87] Thonhauser and Mahan[88] used a ball-and-spring model to study phonon modes in a hexagonally cross-sectioned Si nanowire, demonstrating that the mode boundary conditions consisted of zero stress on surface atoms for acoustic

modes, and zero displacement (or 'clamped' boundary conditions) for optical modes. Their optical eigenmodes are shown in Figure 2.2.12. A tight-binding approach has been used to determine the electronic and phonon properties, and hence the electron-phonon interaction and transport properties, of Si nanowires[89] and field effect transistors based on such nanowires.[90] The mobilities determined in this way were in good agreement with experiment. Atomistic calculations of phonon frequencies, and molecular dynamical simulations of their transport has been performed on Si nanowires by Donadio *et al*.,[91] which confirmed the strong effect of the surface structure and wire diameter on the confined phonons.

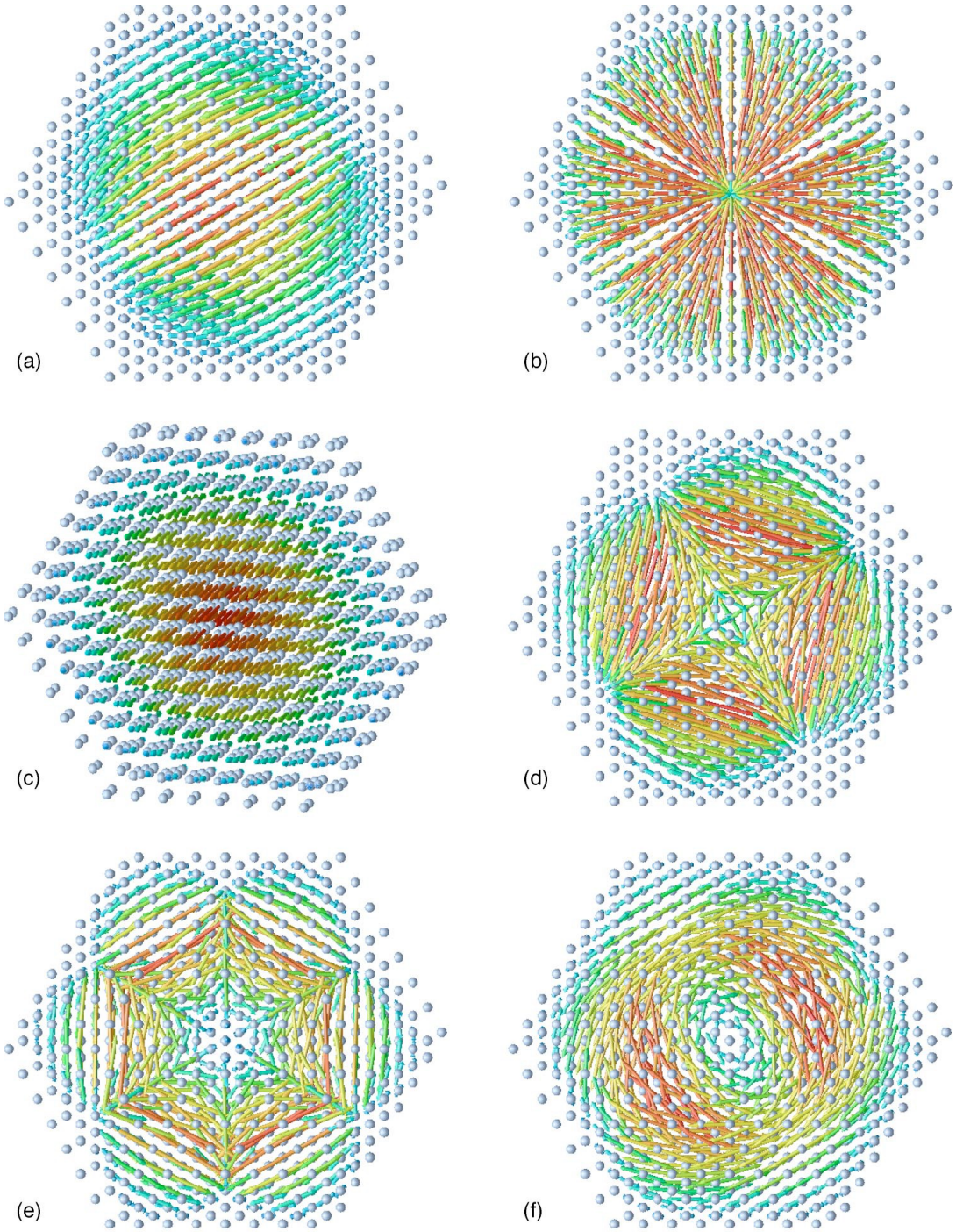

Figure 2.2.12. Optical eigenmodes in a Si nanowire as viewed along the [111] direction.

Finally, Mizuno *et al.*[92] have provided an extensive theoretical study of the possible confined modes in nanowires with square and rectangular cross sections. An example of a calculated phonon dispersion (of a Si nanowire)[88] is given in Figure 2.2.13.

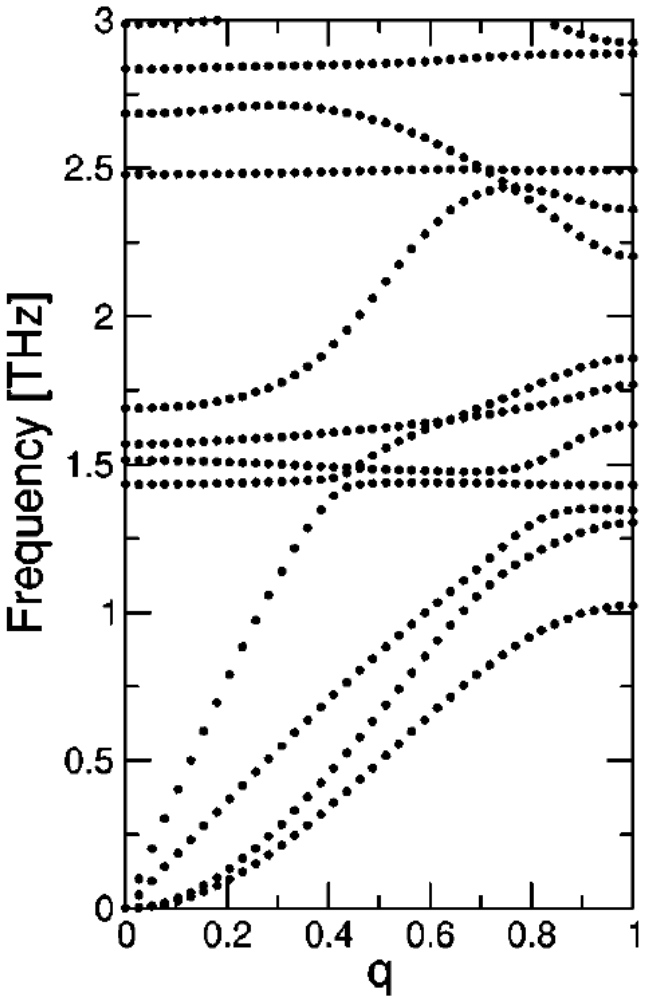

Figure 2.2.13. Phonon dispersion of a hexagonally cross-sectioned Si nanowire.

2.5 Structure and phase transitions in one dimension

The stability of a 1D system is no less surprising than the stability of graphene sheets, which have been the subject of intense research in recent years. One would naively expect thin nanowires to be quite brittle, but it has been shown, by experiment and molecular dynamics simulations, to often not be the case. The mechanical properties of nanowires are quite different to those of the corresponding bulk systems, mainly due to the proportional increase in surface area as size is reduced. Depending on the orientation and thickness of the nanowire, its yield strength can vary widely, but remain significantly higher than that of bulk. This effect is related to energetic barriers to slippage, which occur

due to the stacking of the wire along the axis, as opposed to on the surface. Conversely, the Young's modulus is typically less sensitive to the wire dimensions, but some MD modelling indicates that it can vary for Au nanowires of a particular orientation. For a detailed review of the mechanical properties of nanowires see reference [93].

In the 1930s Peierls pointed out that a 1D metallic chain would be unstable with respect to band gap formation. Considering a linear chain of atoms of separation a, with one electron per atom, according to the Kronig-Penny model considered above, the system will have one half-filled band which would show metallic behaviour. If the atomic spacing were to change so that each atom became simultaneously closer to one neighbour and further from the other, *i.e.* if the symmetry were to spontaneously break as the system dimerises, the increase in elastic energy due to the stretching of one bond may be offset by the energy gain in the formation of a covalent bond of σ character. In this case, the effective lattice spacing is doubled, and the band structure will now contain an energy gap, with a fully occupied valence band. The internal energy of the chain, which includes the thermal energy due to atomic vibrations, will of course depend on the temperature. Below a critical temperature, such lattice distortions will be favourable, while at higher temperatures metallic conductivity will be observed.

Different synthesis procedures lead to different 1D structures, such as wires, tubes, ribbons etc. that typically retain bulk-like atomic arrangements. Once the nanostructure is of sufficiently small diameter (<5-10 nm), however, the bulk-like characteristics are no longer realised. Determining the exact configuration at such sizes is challenging experimentally, leaving theory as the only viable approach at present.

The configuration of a nanowire, even with a given number of atoms, can present a great challenge for structural determination, where large progress is expected from applying global optimisation methods, which, however, has not been realised. The absolute majority of the current modelling is done based on carving a model system from bulk or on construction of new architectures from small predefined nanostructures, usually obtained using global optimisation techniques. In some cases, novel atomic configurations can result from numerical experiments termed uniaxial tensile loading followed by simulated annealing, where a bulk cut is strained in the extended direction and then allowed to relax. For an extended discussion of techniques involved in structure prediction and applied studies see preceding section 2.1.

2.6 Charge and heat transport in ideal systems

The calculation of transport properties in solids is well established, with a variety of approaches available differing in complexity and accuracy. In a metal or semiconductor, electrons (holes) occupy only a fraction of the available conduction (valence) states, which is a necessary condition for energy and momentum transfer. Typically, when treating electron (or hole) carrier transport, the effective mass approximation is applied (see references 94 and 95, whose arguments we follow below), within a one-particle picture, where interactions between carriers are considered negligible and the motion is described either semi-classically, via the Newton's law, or quantum-mechanically, using the Schrödinger equation. Within this approximation, the effect of the periodic crystal potential is such that the carrier moves as if it were a free particle, but with a different mass $m=m^{*}m_{e}$, termed the effective mass. As m^{*} arises from the periodic potential, it can be derived from the crystal band structure.

In section 2.2, we treated electrons as Bloch waves with well-defined quantum numbers $\vec{q}$ (wave numbers). Such a description implies that the electrons delocalise over the entire space. When considering transport, it is often more convenient to describe electrons as particles with well-defined positions and/or velocities/(quasi-)momenta (subject, however, to the Heisenberg uncertainty principle), which can be achieved by representing electrons as packets (groups) of Bloch waves, moving with a group velocity

$$\vec{v}=\nabla_{\vec{q}}\omega(\vec{q})=\frac{1}{\hbar}\nabla_{\vec{q}}E(\vec{q}), \quad (2.2.12)$$

where $E(\vec{q})$, is the $\vec{q}$-space structure (dispersion) for the particular conduction band. Given an applied electric field, $\vec{E}$, the work done on the particle of charge $-e$ is given by

$$\delta E=-e\vec{E}\cdot\vec{v}\,\delta t, \quad (2.2.13)$$

From equation (2.2.12) we can derive

$$\delta E=\hbar\,\vec{v}\cdot\delta\vec{q}, \quad (2.2.14)$$

and combining (2.2.13) and (2.2.14) we find

$$\hbar\dot{\vec{q}}=-e\vec{E}. \quad (2.2.15)$$

Taking the time derivative of Equation (2.2.12), for each component i (¿x, y, z)

$$\dot{v_i}=\frac{1}{\hbar}\sum_j \frac{\partial^2 E}{\partial q_i \partial q_j}\dot{q}_j, \quad (2.2.16)$$

from which, taking Equation (2.2.15), we derive

$$\dot{\vec{v}} = \frac{1}{\hbar^2} \sum_j \frac{\partial^2 E}{\partial q_i \partial q_j} (-e\vec{E}), \tag{2.2.17}$$

Equation (2.2.16) is analogous to the classical Newton's equation, with mass given by the tensor:

$$\left(\frac{1}{m^*}\right)_{ij} = \frac{1}{\hbar^2} \sum_j \frac{\partial^2 E}{\partial q_i \partial q_j}, \tag{2.2.18}$$

which is symmetric and can therefore be transformed to principle axes.

At equilibrium, there is no net displacement $\vec{r}$ of carriers. One then considers the case when there is an applied field $\vec{E}$, which accelerates the particle subject to occasional scattering processes that in turn slow it down (if such scattering processes were not present, the acceleration due to $\vec{E}$ would result in an infinite velocity and hence infinite current). Thus naturally emerge two time scales: over one, the particles accelerate between collisions, and over the other, subject to many collisions the particles move with an average constant velocity – see below. The slowing down, or drag will be proportional to the particle velocity and inversely proportional to the average time τ between collisions. Such a drag force is also proportional to the particle mass, which affects the acceleration between the collisions and therefore the average velocity. The appropriate Newton's equation (over the longer time scale) is:

$$m^* \frac{d^2\vec{r}}{dt^2} + \frac{m^*}{\tau} \frac{d\vec{r}}{dt} = -e\vec{E}, \tag{2.2.19}$$

where τ is termed the scattering relaxation time. As the particle is accelerated, the velocity and hence the drag increase until a steady state is achieved, in which the drag term counters precisely the applied field so that on average the particles move with a drift velocity given by

$$\vec{v}_d = -e\vec{E}\frac{\tau}{m^*}, \tag{2.2.20}$$

from which the current density $\vec{J} = -ne\vec{v}_d$ (n is the charge carrier density) and, hence, the conductivity σ can be determined (from $\vec{J} = \sigma\vec{E}$, and a scalar conductivity is defined as one of the principal values of tensor σ). A more useful property, however, to calculate is the mobility μ, defined as the constant (tensor) of proportionality between $\vec{v}_d$ and $\vec{E}$ (*i.e.* $\vec{v}_d = \mu\vec{E}$), as it is independent of the carrier density, which can vary widely in semiconductors with temperature or doping level. We then have:

$$\mu = e\frac{\tau}{m^*}, \tag{2.2.21}$$

As shown above, *m** can be derived from the crystal band structure (it could also be taken from experiment, or used as a parameter to be fitted to other experimental results). The complications to determining μ come from the property τ.

The simplest approach is to treat τ as a constant, derived phenomenologically, *e.g.* from measurements of resistivities, which, however, limits the predictability of the model. As we consider transport in the periodic system, scattering occurs from breaks in periodicity, i.e. lattice vibrations, defects, and surfaces/interfaces. Each of these scattering processes has a characteristic rate τ_i, the reciprocal of which is the scattering rate R_i,

which, according to Matthiessen's rule, can be summed together to determine a total scattering rate R. Different approaches can be taken to calculate these scattering rates, with the most accurate being the determination of appropriate wave functions and applying Fermi's Golden Rule, including the relevant scattering potential (*e.g.* electron-phonon, electron-electron, screened Coulomb, *etc*.).

The mobility was introduced in order to characterise the transport properties of an average single carrier, which in turn are determined by the statistical properties of scatterers. For example, the concentration of charged impurities in a system can be considered as constant over a wide range of temperatures above a certain threshold, whereas the number of acoustic vibrations is strongly dependent on temperature (following Bose-Einstein statistics). The effect of temperature on the mobility then consists of two contributions: the number of scattering centres themselves, and the energy-dependent scattering of the carriers (which will be reflected in the form of the wave functions and scattering potential used in Fermi's Golden Rule). Such temperature effects are of a more fundamental nature than those that occur purely based on the variation of carrier density.

Heat transfer involves the redistribution of thermal energy from one region of the system to a neighbouring region, in which the population (energy distribution) of local electronic states and/or phonon modes is modified. In contrast to charge transport, therefore, two mechanisms contribute to heat transport: electronic heat transport and heat transport by phonons. The electronic contribution dominates in metals and degenerate semiconductors. For a temperature gradient, ∇T, we have

$$\vec{J}_{th} = -\kappa \nabla T, \tag{2.2.22}$$

where $\vec{J}_{th}$ is the total thermal current (i.e. the net thermal energy transported across unit area in unit time), κ is the thermal conductivity, and the negative sign indicates transport from high to low *T*. Apart from mutual scattering between the two types of particles involved, the two different contributions can be determined separately and summed together, *i.e.* $\kappa = \kappa_e + \kappa_p$, where κ_e and κ_p are the thermal conductivities associated with electrons and phonons, respectively.

As the thermal energy in the system is determined by the internal energy with contributions from the potential, vibrational and charge carrier terms, a key property to consider is the specific heat capacity $c_v = \partial U / \partial T$, where U is the internal energy. Using the chain rule we have $\nabla U = c_v \nabla T$, which, from Eq. (2.2.22) and the fact that thermal currents relate to changes in *U* as a function of position, indicates that c_v will appear in an expression for κ. For electrons, we have

$$\kappa_e = \frac{1}{3} v^2 \tau c_v, \tag{2.2.23}$$

where v is the average (drift) velocity.

For phonons, the situation is somewhat more complicated. Phonons, which are the quanta of harmonic lattice vibrational modes, are derived under the harmonic approximation, while thermal transport effects are anharmonic in

nature. Similar to how we treated electrons above, we can build a picture of phonon Bloch wave packets propagating through the system, redistributing the thermal energy by scattering mechanisms, in which the initial packet can annihilate (reducing the phonon population at the source) while a new phonon packet(s) is created (increasing the local – sink – phonon population). We therefore, as a first approximation, consider phonons as particles that can interact with each other, with a drift velocity v_{ph} and average scattering times τ_{ph}, which are primarily determined by interactions with other phonons, electrons, or defects. The heat capacity in this case can be obtained within the usual quasiharmonic approximation. This description yields an analogous expression for κ_p to that given in Eq. (2.2.23) for κ_e. The relevant τ can be calculated in a similar fashion to that discussed previously for the charge carriers. Such calculations are key to determining the highly significant thermoelectric properties of materials.[96]

Transport in 1D systems is different from what we know for the bulk systems as

(i) the underlying one-particle spectra, both electron and phonon, have essential 1D features from effects such as quantum confinement, symmetry breaking (see sections 2.2.3- 2.2.5), *etc*. with a direct impact on the carrier concentrations on one hand and on the relaxation times on the other;

(ii) the surface to bulk ratio becomes significant and, for example, surface states could be either dominant scatterers or conduction channels, which would determine the values of the relaxation time,

but would also require consideration of the current inhomogeneity in the dimensions normal to the wire axis;

(iii) the current may display intrinsic quantum properties if the wire dimensions are such that the length of the wire is less than the mean free path of the charge carriers, so that scattering events become unlikely and a ballistic transport occurs.

Next, we will consider a few example studies of realistic 1D systems, for which both theory and modelling have been successfully applied. All three factors peculiar to 1D may combine or remain hidden but invariably at least one would play an important role.

The electron mobility in a Si nanowire has been modelled as affected by fluctuations in the electron waves due to the surface roughness and by electron-phonon scattering via differing intra- and intervalley mechanisms by Jin *et al*.[97] The electron wave functions were calculated by self-consistently solving the Schrödinger and Poisson equations, with 1D effects leading to electron energy subband formation. The surface effects introduced in the model included the Coulomb potential due to charge fluctuations and surface polarisation, and the resultant non-parabolicity of the energy subbands. Fermi's Golden Rule is used to calculate the scattering rates from the different scattering mechanisms (surface roughness, Coulomb, and phonon) and a Kubo-Greenwood formulism is used to determine the mobility. In Fig 2.2.14, the resulting mobility as a function of wire diameter d and effective electric field E_{eff} perpendicular to the wire axis is shown, highlighting the different contributions from the different scattering mechanisms. As expected, the surface effects dominate for smaller d.

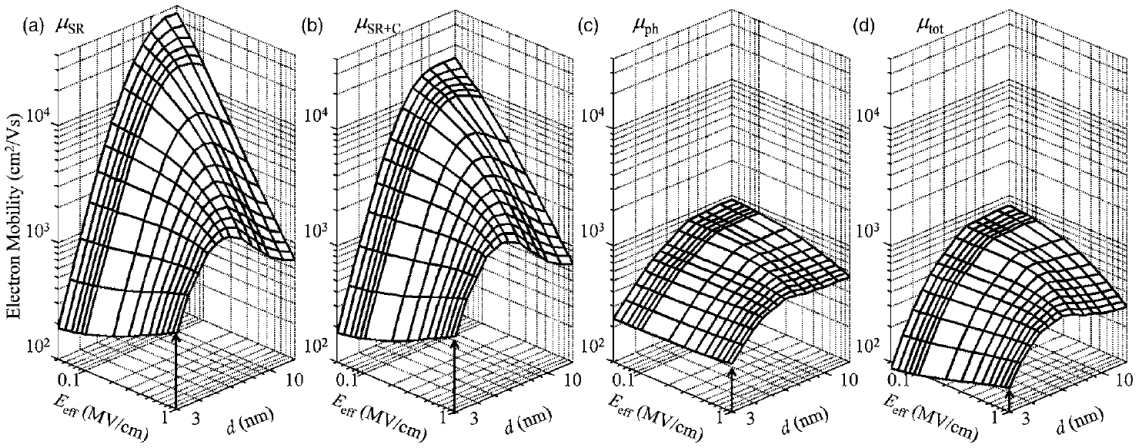

Figure 2.2.14. Calculated mobility as a function of wire diameter and effective field perpendicular to wire axis, highlighting the different contributions from surface roughness, Coulomb, and phonon scattering.

In Ref. 98, Zou and Balandin calculate the heat conduction due to phonon transport in a Si nanowire. The conductivity is assumed to be dominated by acoustic phonon transport. The effect of confinement on the phonon frequencies and scattering due to phonon-phonon interactions (including three-phonon *Umklapp*, or flip-over processes and phonon mass differences), boundary (*i.e.* surface) effects, and electron-phonon interactions are included in the model. They found that confinement significantly softened the acoustic mode dispersion, while boundary scattering, which dominated over a wide range of phonon frequencies, led to approximately an order of magnitude reduction in the thermal conductivity, relative to bulk. Even without boundary scattering, they found significant reductions in the thermal conductivity, indicating the important role of quantum confinement in the transport properties.

When determining the scattering of electrons by phonons (or *vice versa*), the interaction Hamiltonian is characterised by parameters known as deformation potentials (relating the degree to which the electronic energies change due to the interaction), which depend on the strain introduced by the ionic motion within the phonon mode. As a result, different phonons (LA, TA, LO,

TO) have different deformation potentials associated with them. Calculations of electronic structure as a function of strain introduced by phonons can be used to determine the deformation potentials, which are material specific. Murphy-Armando *et al*.[99] have calculated how the electron-phonon interaction in Si changes for the case of 1D nanowires, in comparison to bulk. Using first-principles methods to determine the electronic structure, they derived the deformation potentials for different wire thicknesses and orientations, considering termination in the confinement directions by H atoms and by hydroxyls. It was found that, although the surface structure and chemistry strongly modified the band structure, they had little effect on the deformation potentials. The reduced dimensionality of the wire, however, was found to alter the deformation potentials fundamentally, leading to them being strongly dependent on the strain direction. In addition, the orientation of the wire affected the deformation potentials, with [110] wires being more anisotropic than [100] and bulk, resulting in suppression of breathing mode scattering and increased electron mobility.

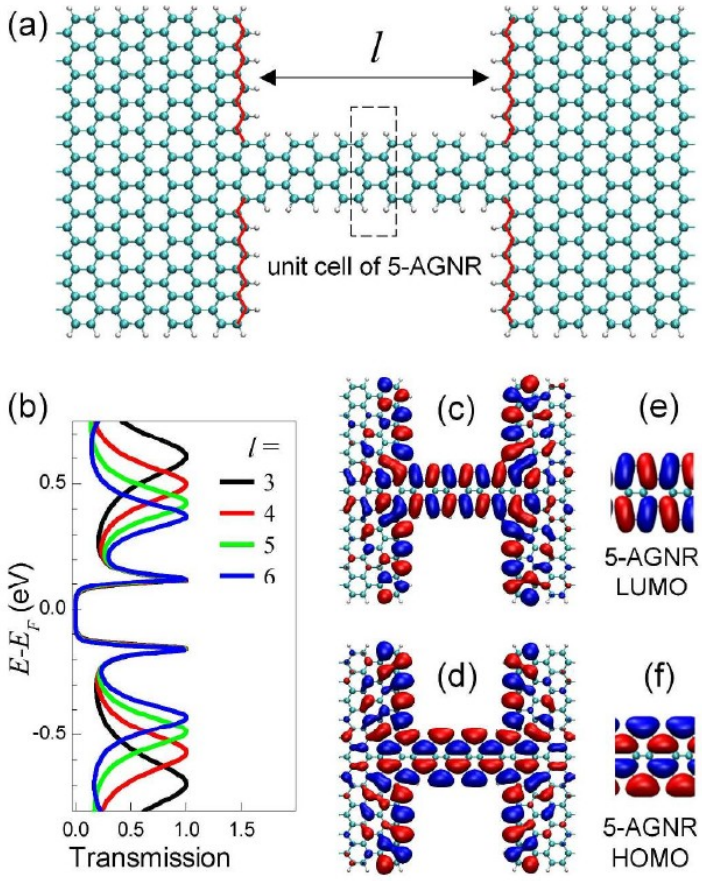

Figure 2.2.15. A computational transmission model for a molecular wire.

In reference to point (iii) above, an extreme example is provided by so-called 1D molecular wires, in which, for very short lengths (< 5 nm), electron transport occurs mainly by quantum tunnelling effects, while at longer lengths by a thermally induced 'hopping'. An example is shown in Figure 2.2.15. We do not discuss in detail the transport in such systems, as it is debatable as to whether they truly are 1D (as opposed to 0D nanostructures). For a recent review on calculations of electron transport in such systems, see reference 100 and further discussion in this book.

2.7 Defect states

Similar to extended 3D systems, the structure in 1D can order at different length scales. Irrespective of a long-range order, or “crystallinity”, any extended solid system with homogeneous distribution of atoms (characterised by constant

linear density) is expected to exhibit some form of a short range order, with atoms distributed around any given centre in a pattern, which would be repeated throughout the system. Breaking such a pattern gives rise to point defects, intrinsic in the form of vacancies, interstitial atoms, and antisites (arsenic occupying for example a gallium site in GaAs); extrinsic, or impurities occupying regular or interstitial sites (*e.g.* silicon at a gallium site in GaAs); and their complexes. Following the same entropic or free energy arguments exploited in the theory of phase stability, finite concentrations of intrinsic defects are unavoidable in any given macroscopic sample, whereas impurities would be introduced during synthesis as the source material is practically never absolutely pure. Importantly, however, both intrinsic and extrinsic defects could be introduced into the system of interest intentionally to modify physical and chemical properties of the material, *e.g.* its optical spectra, resistivity or (photo-)catalytic activity. By disrupting the atomic structure, point defects introduce localised electron and vibrational states and act as scatterers for free charge carriers and phonons.

Modelling of defect states in nanowires is still in its infancy and we refer the interested reader to two recent publications for pertinent examples and a more detailed review of the topic.[101-104]

2.8 Conclusions

In conclusion we would like to point the interested reader to the follow up chapters in this book, where a number of topics, which we only touched are discussed in depth. There remain in this field many open questions and problems to attack by new researchers, of which an especially curious one is: why do one dimensional systems exist, can be made and persist for macroscopic times, at all? Accurate predictive modelling of nonequilibrium processes in such complex

systems is only beginning to be developed and promises novel exciting discoveries.

Acknowledgements

For many useful insights, discussions and support we are indebted to our colleagues and collaborators S.T. Bromley, C.R.A. Catlow, A. Chutia, M.R. Farrow, R. Galvelis, N. Jiang, T. Lazauskas, Z. Raza, D. O. Scanlon, S. A. Shevlin, A. Walsh, and S.M. Woodley.

References

1 Bertness, K. A. *et al.* Catalyst-free growth of GaN nanowires. *Journal of Elec Materi* **35**, 576-580, doi:10.1007/s11664-006-0102-4 (2006).
2 Kim, D. K. *et al.* Spinel LiMn2O4 Nanorods as Lithium Ion Battery Cathodes. *Nano Letters* **8**, 3948-3952, doi:10.1021/nl8024328 (2008).
3 Chen, X. J. *et al.* Catalyst-free growth of high-optical quality GaN nanowires by metal-organic vapor phase epitaxy. *Applied Physics Letters* **99**, 251910, doi:doi:http://dx.doi.org/10.1063/1.3671365 (2011).
4 Prado-Gonjal, J., Schmidt, R. & Morán, E. Microwave-Assisted Routes for the Synthesis of Complex Functional Oxides. *Inorganics* **3**, 101 (2015).
5 Nakane, K. & Ogata, N. *Photocatalyst Nanofibers Obtained by Calcination of Organic-Inorganic Hybrids*. (2010).
6 Treutlein, P., Hunger, D., Camerer, S., Hänsch, T. W. & Reichel, J. Bose-Einstein Condensate Coupled to a Nanomechanical Resonator on an Atom Chip. *Physical Review Letters* **99**, 140403 (2007).
7 Curreli, M. *et al.* Selective Functionalization of In2O3 Nanowire Mat Devices for Biosensing Applications. *Journal of the American Chemical Society* **127**, 6922-6923, doi:10.1021/ja0503478 (2005).
8 Céline, M. *et al.* Improvements in purification of silver nanowires by decantation and fabrication of flexible transparent electrodes. Application to capacitive touch sensors. *Nanotechnology* **24**, 215501 (2013).
9 Wang, N. *et al.* Piezotronic-Effect Enhanced Drug Metabolism and Sensing on a Single ZnO Nanowire Surface with the Presence of Human Cytochrome P450. *ACS Nano* **9**, 3159-3168, doi:10.1021/acsnano.5b00142 (2015).
10 Myung-Gyu, K., Henri, J. L. & Fred, S. Stable field emission from nanoporous silicon carbide. *Nanotechnology* **24**, 065201 (2013).
11 Hill, M. T. *et al.* Lasing in metal-insulator-metal sub-wavelength plasmonic waveguides. *Optics Express* **17**, 11107-11112 (2009).
12 Feng, Y. & Zheng, X. Plasma-Enhanced Catalytic CuO Nanowires for CO Oxidation. *Nano Letters* **10**, 4762-4766, doi:10.1021/nl1034545 (2010).
13 He, Y. *et al.* Highly Luminescent Water-Dispersible Silicon Nanowires for Long-Term Immunofluorescent Cellular Imaging. *Angewandte Chemie International Edition* **50**, 3080-3083, doi:10.1002/anie.201100482 (2011).
14 Wang, Q., Sun, J. & Liu, H. in *Nanowires - Implementations and Applications* (ed Abbas Hashim) Ch. 4, 59-98 (InTech, 2011).
15 Shalin, A. S., Ginzburg, P., Belov, P. A., Kivshar, Y. S. & Zayats, A. V. Nano-opto-mechanical effects in plasmonic waveguides. *Laser & Photonics Reviews* **8**, 131-136, doi:10.1002/lpor.201300109 (2014).

16 Wang, X., Tian, W., Liao, M., Bando, Y. & Golberg, D. Recent advances in solution-processed inorganic nanofilm photodetectors. *Chemical Society Reviews* **43**, 1400-1422, doi:10.1039/c3cs60348b (2014).
17 Guo, C. X., Dong, Y., Yang, H. B. & Li, C. M. Graphene Quantum Dots as a Green Sensitizer to Functionalize ZnO Nanowire Arrays on F-Doped SnO2 Glass for Enhanced Photoelectrochemical Water Splitting. *Advanced Energy Materials* **3**, 997-1003, doi:10.1002/aenm.201300171 (2013).
18 Kim, S.-K. *et al.* Design of Nanowire Optical Cavities as Efficient Photon Absorbers. *ACS Nano* **8**, 3707-3714, doi:10.1021/nn5003776 (2014).
19 Sun, C., Shi, J. & Wang, X. Fundamental study of mechanical energy harvesting using piezoelectric nanostructures. *Journal of Applied Physics* **108**, 034309, doi:doi:http://dx.doi.org/10.1063/1.3462468 (2010).
20 Cheran, L.-E., Cheran, A. & Thompson, M. in *Advanced Synthetic Materials in Detection Science* 1-25 (The Royal Society of Chemistry, 2014).
21 Pennelli, G. Review of nanostructured devices for thermoelectric applications. *Beilstein Journal of Nanotechnology* **5**, 1268-1284, doi:10.3762/bjnano.5.141 (2014).
22 Hofmann, C. E. & Atwater, H. A. in *SPIE* 1-3 (2008).
23 Yan, L., Zhang, J., Lee, C.-S. & Chen, X. Micro- and Nanotechnologies for Intracellular Delivery. *Small* **10**, 4487-4504, doi:10.1002/smll.201401532 (2014).
24 Feng, P., Shao, F., Shi, Y. & Wan, Q. Gas Sensors Based on Semiconducting Nanowire Field-Effect Transistors. *Sensors* **14**, 17406 (2014).
25 Brian, P., Carlos, O. A., Chang-Hee, C. & Ritesh, A. Tailoring light–matter coupling in semiconductor and hybrid-plasmonic nanowires. *Reports on Progress in Physics* **77**, 086401 (2014).
26 Tang, J. & Wang, K. L. Electrical spin injection and transport in semiconductor nanowires: challenges, progress and perspectives. *Nanoscale* **7**, 4325-4337, doi:10.1039/c4nr07611g (2015).
27 Lim, Z. H., Chia, Z. X., Kevin, M., Wong, A. S. W. & Ho, G. W. A facile approach towards ZnO nanorods conductive textile for room temperature multifunctional sensors. *Sensors and Actuators B: Chemical* **151**, 121-126, doi:http://dx.doi.org/10.1016/j.snb.2010.09.037 (2010).
28 Zou, D., Lv, Z., Cai, X. & Hou, S. Macro/microfiber-shaped electronic devices. *Nano Energy* **1**, 273-281, doi:http://dx.doi.org/10.1016/j.nanoen.2012.01.005 (2012).
29 Tian, B. *et al.* Macroporous nanowire nanoelectronic scaffolds for synthetic tissues. *Nat Mater* **11**, 986-994, doi:http://www.nature.com/nmat/journal/v11/n11/abs/nmat3404.html#supplementary-information (2012).
30 Kheireddin, B. A., Narayanunni, V. & Akbulut, M. Influence of Shearing Surface Topography on Frictional Properties of ZnS Nanowire-Based Lubrication System across Ductile Surfaces. *Journal of Tribology* **134**, 022001-022001, doi:10.1115/1.4005891 (2012).
31 Cademartiri, L. & Ozin, G. A. Ultrathin Nanowires - A Materials Chemistry Perspective. *Advanced Materials* **21**, 1013-1020, doi:10.1002/adma.200801836 (2009).
32 Li, H. *et al.* One-Dimensional CdS Nanostructures: A Promising Candidate for Optoelectronics. *Advanced Materials* **25**, 3017-3037, doi:10.1002/adma.201300244 (2013).
33 Harris, P. J. F. *Carbon Nanotube Science*. (Cambridge University Press, 2009).
34 Javey, A. & Kong, J. Vol. 1 267 (Springer US, 2009).

35 Tománek, D. in *Buckyballs, nanotubes, graphene and beyond* 93 (Morgan & Claypool Publishers, San Rafael, CA, 2014).
36 Li, C. P. *et al.* Ultrafine and uniform silicon nanowires grown with zeolites. *Chemical Physics Letters* **365**, 22-26, doi:http://dx.doi.org/10.1016/S0009-2614(02)01375-1 (2002).
37 Gurwitz, R., Tuboul, G., Shikler, B. & Shalish, I. High-temperature gold metallization for ZnO nanowire device on a SiC substrate. *Journal of Applied Physics* **111**, doi:12430710.1063/1.4729802 (2012).
38 Perillat-Merceroz, G., Thierry, R., Jouneau, P. H., Ferret, P. & Feuillet, G. Compared growth mechanisms of Zn-polar ZnO nanowires on O-polar ZnO and on sapphire. *Nanotechnology* **23**, doi:12570210.1088/0957-4484/23/12/125702 (2012).
39 Khaletskaya, K. *et al.* Integration of Porous Coordination Polymers and Gold Nanorods into Core–Shell Mesoscopic Composites toward Light-Induced Molecular Release. *Journal of the American Chemical Society* **135**, 10998-11005, doi:10.1021/ja403108x (2013).
40 Volosskiy, B. *et al.* Metal-Organic Framework Templated Synthesis of Ultrathin, Well-Aligned Metallic Nanowires. *ACS Nano* **9**, 3044-3049, doi:10.1021/nn5072446 (2015).
41 Ewald, P. P. The calculation of optical and electrostatic grid potential. *Ann. Phys.-Berlin* **64**, 253-287 (1921).
42 Mertins, F. Potentials in low-dimensional and semi-infinite crystals. *Ann. Phys.-Berlin* **8**, 261-300, doi:10.1002/(sici)1521-3889(199904)8:4<261::aid-andp261>3.3.co;2-a (1999).
43 Minary, P., Morrone, J. A., Yarne, D. A., Tuckerman, M. E. & Martyna, G. J. Long range interactions on wires: A reciprocal space based formalism. *Journal of Chemical Physics* **121**, 11949-11956, doi:10.1063/1.1806403 (2004).
44 Saunders, V. R., Freyriafava, C., Dovesi, R. & Roetti, C. ON THE ELECTROSTATIC POTENTIAL IN LINEAR PERIODIC POLYMERS. *Computer Physics Communications* **84**, 156-172, doi:10.1016/0010-4655(94)90209-7 (1994).
45 Castro, A., Rasanen, E. & Rozzi, C. A. Exact Coulomb cutoff technique for supercell calculations in two dimensions. *Physical Review B* **80**, doi:10.1103/PhysRevB.80.033102 (2009).
46 Abarenko.Iv & Heine, V. MODEL POTENTIAL FOR POSITIVE IONS. *Philosophical Magazine* **12**, 529-&, doi:10.1080/14786436508218898 (1965).
47 Kleinman, L. & Bylander, D. M. Efficacious Form for Model Pseudopotentials. *Physical Review Letters* **48**, 1425-1428 (1982).
48 Austin, B. J., Sham, L. J. & Heine, V. GENERAL THEORY OF PSEUDOPOTENTIALS. *Physical Review* **127**, 276-&, doi:10.1103/PhysRev.127.276 (1962).
49 Hamann, D. R., Schluter, M. & Chiang, C. NORM-CONSERVING PSEUDOPOTENTIALS. *Physical Review Letters* **43**, 1494-1497, doi:10.1103/PhysRevLett.43.1494 (1979).
50 Wadt, W. R. & Hay, P. J. Ab initio effective core potentials for molecular calculations. Potentials for main group elements Na to Bi. *The Journal of Chemical Physics* **82**, 284-298, doi:doi:http://dx.doi.org/10.1063/1.448800 (1985).
51 Martin, R. M. *Electronic structure. Basic theory and practical methods*. (Cambridge University Press, 2004).

52 Zhao, Y., Lynch, B. J. & Truhlar, D. G. Doubly hybrid meta DFT: New multi-coefficient correlation and density functional methods for thermochemistry and thermochemical kinetics. *J. Phys. Chem. A* **108**, 4786-4791, doi:10.1021/jp049253v (2004).
53 Kresse, G. & Furthmüller, J. Efficiency of ab-initio total energy calculations for metals and semiconductors using a plane-wave basis set. *Computational Materials Science* **6**, 15-50, doi:http://dx.doi.org/10.1016/0927-0256(96)00008-0 (1996).
54 Kresse, G. & Furthmüller, J. Efficient iterative schemes for ab initio total-energy calculations using a plane-wave basis set. *Physical Review B* **54**, 11169-11186 (1996).
55 Kresse, G. & Hafner, J. Ab initio molecular dynamics for liquid metals. *Physical Review B* **47**, 558-561 (1993).
56 Kresse, G. & Hafner, J. Ab initio molecular-dynamics simulation of the liquid-metal–amorphous-semiconductor transition in germanium. *Physical Review B* **49**, 14251-14269 (1994).
57 Blöchl, P. E. Projector augmented-wave method. *Physical Review B* **50**, 17953-17979 (1994).
58 Ernzerhof, M. & Scuseria, G. E. Assessment of the Perdew–Burke–Ernzerhof exchange-correlation functional. *The Journal of Chemical Physics* **110**, 5029-5036, doi:doi:http://dx.doi.org/10.1063/1.478401 (1999).
59 Perdew, J. P., Burke, K. & Ernzerhof, M. Generalized Gradient Approximation Made Simple. *Physical Review Letters* **77**, 3865 (1996).
60 Perdew, J. P. *et al.* Restoring the Density-Gradient Expansion for Exchange in Solids and Surfaces. *Physical Review Letters* **100**, 136406 (2008).
61 Adamo, C. & Barone, V. Toward reliable density functional methods without adjustable parameters: The PBE0 model. *The Journal of Chemical Physics* **110**, 6158-6170, doi:doi:http://dx.doi.org/10.1063/1.478522 (1999).
62 Gnani, E. *et al.* Band-Structure Effects in Ultrascaled Silicon Nanowires. *Electron Devices, IEEE Transactions on* **54**, 2243-2254, doi:10.1109/ted.2007.902901 (2007).
63 Nehari, K. *et al.* Influence of band structure on electron ballistic transport in silicon nanowire MOSFET's: An atomistic study. *Solid-State Electronics* **50**, 716-721, doi:http://dx.doi.org/10.1016/j.sse.2006.03.041 (2006).
64 Scheel, H., Reich, S. & Thomsen, C. Electronic band structure of high-index silicon nanowires. *Physica Status Solidi (b)* **242**, 2474-2479, doi:10.1002/pssb.200541133 (2005).
65 Nolan, M., O'Callaghan, S., Fagas, G., Greer, J. C. & Frauenheim, T. Silicon Nanowire Band Gap Modification. *Nano Letters* **7**, 34-38, doi:10.1021/nl061888d (2007).
66 Hong, K.-H., Kim, J., Lee, S.-H. & Shin, J. K. Strain-Driven Electronic Band Structure Modulation of Si Nanowires. *Nano Letters* **8**, 1335-1340, doi:10.1021/nl0734140 (2008).
67 Pistol, M. E. & Pryor, C. E. Band structure of core-shell semiconductor nanowires. *Physical Review B* **78**, 115319 (2008).
68 Lind, E., Persson, M. P., Niquet, Y.-M. & Wernersson, L. E. Band Structure Effects on the Scaling Properties of [111] InAs Nanowire MOSFETs. *Electron Devices, IEEE Transactions on* **56**, 201-205, doi:10.1109/ted.2008.2010587 (2009).
69 Ketterer, B., Heiss, M., Uccelli, E., Arbiol, J. & Fontcuberta i Morral, A. Untangling the Electronic Band Structure of Wurtzite GaAs Nanowires by Resonant Raman Spectroscopy. *ACS Nano* **5**, 7585-7592, doi:10.1021/nn202585j (2011).

70 Yeom, H. W., Kim, Y. K., Lee, E. Y., Ryang, K. D. & Kang, P. G. Robust One-Dimensional Metallic Band Structure of Silicide Nanowires. *Physical Review Letters* **95**, 205504 (2005).
71 Brus, L. Luminescence of Silicon Materials: Chains, Sheets, Nanocrystals, Nanowires, Microcrystals, and Porous Silicon. *The Journal of Physical Chemistry* **98**, 3575-3581, doi:10.1021/j100065a007 (1994).
72 Perera, S. *et al.* Probing valence band structure in wurtzite InP nanowires using excitation spectroscopy. *Applied Physics Letters* **97**, 023106, doi:doi:http://dx.doi.org/10.1063/1.3463036 (2010).
73 Lu, W., Xiang, J., Timko, B. P., Wu, Y. & Lieber, C. M. One-dimensional hole gas in germanium/silicon nanowire heterostructures. *Proceedings of the National Academy of Sciences of the United States of America* **102**, 10046-10051, doi:10.1073/pnas.0504581102 (2005).
74 Togo, A., Oba, F. & Tanaka, I. First-principles calculations of the ferroelastic transition between rutile-type and ${\text{CaCl}}_{2}$-type ${\text{SiO}}_{2}$ at high pressures. *Physical Review B* **78**, 134106 (2008).
75 Lee, K.-Y. *et al.* Evolution of optical phonons in CdS nanowires, nanobelts, and nanosheets. *Applied Physics Letters* **91**, 201901, doi:doi:http://dx.doi.org/10.1063/1.2806937 (2007).
76 Wang, R.-p. *et al.* Raman spectral study of silicon nanowires: High-order scattering and phonon confinement effects. *Physical Review B* **61**, 16827-16832 (2000).
77 Adu, K. W., Gutiérrez, H. R., Kim, U. J., Sumanasekera, G. U. & Eklund, P. C. Confined Phonons in Si Nanowires. *Nano Letters* **5**, 409-414, doi:10.1021/nl0486259 (2005).
78 Adu, K. W., Xiong, Q., Gutierrez, H. R., Chen, G. & Eklund, P. C. Raman scattering as a probe of phonon confinement and surface optical modes in semiconducting nanowires. *Applied Physics A* **85**, 287-297, doi:10.1007/s00339-006-3716-8 (2006).
79 Shi, W. S., Zheng, Y. F., Wang, N., Lee, C. S. & Lee, S. T. Oxide-assisted growth and optical characterization of gallium-arsenide nanowires. *Applied Physics Letters* **78**, 3304-3306, doi:doi:http://dx.doi.org/10.1063/1.1371966 (2001).
80 Spirkoska, D., Abstreiter, G. & Morral, A. F. i. Size and environment dependence of surface phonon modes of gallium arsenide nanowires as measured by Raman spectroscopy. *Nanotechnology* **19**, 435704 (2008).
81 Shi, W. *et al.* Laser Ablation Synthesis and Optical Characterization of Silicon Carbide Nanowires. *Journal of the American Ceramic Society* **83**, 3228-3230, doi:10.1111/j.1151-2916.2000.tb01714.x (2000).
82 Chen, C.-C. *et al.* Catalytic Growth and Characterization of Gallium Nitride Nanowires. *Journal of the American Chemical Society* **123**, 2791-2798, doi:10.1021/ja0040518 (2001).
83 Lo, S. S. *et al.* Charge Carrier Trapping and Acoustic Phonon Modes in Single CdTe Nanowires. *ACS Nano* **6**, 5274-5282, doi:10.1021/nn3010526 (2012).
84 Weber, C. *et al.* Probing Confined Phonon Modes by Transport through a Nanowire Double Quantum Dot. *Physical Review Letters* **104**, 036801 (2010).
85 Boukai, A. I. *et al.* Silicon nanowires as efficient thermoelectric materials. *Nature* **451**, 168-171, doi:http://www.nature.com/nature/journal/v451/n7175/suppinfo/nature06458_S1.html (2008).

86 Chen, R. *et al.* Thermal Conductance of Thin Silicon Nanowires. *Physical Review Letters* **101**, 105501 (2008).
87 Richter, H., Wang, Z. P. & Ley, L. The one phonon Raman spectrum in microcrystalline silicon. *Solid State Communications* **39**, 625-629, doi:http://dx.doi.org/10.1016/0038-1098(81)90337-9 (1981).
88 Thonhauser, T. & Mahan, G. D. Phonon modes in Si [111] nanowires. *Physical Review B* **69**, 075213 (2004).
89 Zhang, W., Delerue, C., Niquet, Y.-M., Allan, G. & Wang, E. Atomistic modeling of electron-phonon coupling and transport properties in n-type [110] silicon nanowires. *Physical Review B* **82**, 115319 (2010).
90 Luisier, M. & Klimeck, G. Atomistic full-band simulations of silicon nanowire transistors: Effects of electron-phonon scattering. *Physical Review B* **80**, 155430 (2009).
91 Donadio, D. & Galli, G. Atomistic Simulations of Heat Transport in Silicon Nanowires. *Physical Review Letters* **102**, 195901 (2009).
92 Seiji, M. & Norihiko, N. Acoustic phonon modes and dispersion relations of nanowire superlattices. *Journal of Physics: Condensed Matter* **21**, 195303 (2009).
93 Li, H. & Sun, F. in *Nanowires - Recent Advances* (ed Xihong Peng) Ch. 16, 371-394 (InTech, 2012).
94 Ibach, H. & Lüth, H. in *Solid-State Physics* Ch. 4, 83-112 (Springer Berlin Heidelberg, 2009).
95 Yu, P. Y. & Cardona, M. *Fundamentals of Semiconductors*. 3rd edn, (Springer, 2005).
96 Skelton, J. M., Parker, S. C., Togo, A., Tanaka, I. & Walsh, A. Thermal physics of the lead chalcogenides PbS, PbSe, and PbTe from first principles. *Physical Review B* **89**, doi:10.1103/PhysRevB.89.205203 (2014).
97 Jin, S., Fischetti, M. V. & Tang, T.-w. Modeling of electron mobility in gated silicon nanowires at room temperature: Surface roughness scattering, dielectric screening, and band nonparabolicity. *Journal of Applied Physics* **102**, 083715, doi:doi:http://dx.doi.org/10.1063/1.2802586 (2007).
98 Zou, J. & Balandin, A. Phonon heat conduction in a semiconductor nanowire. *Journal of Applied Physics* **89**, 2932-2938, doi:doi:http://dx.doi.org/10.1063/1.1345515 (2001).
99 Murphy-Armando, F., Fagas, G. & Greer, J. C. Deformation Potentials and Electron−Phonon Coupling in Silicon Nanowires. *Nano Letters* **10**, 869-873, doi:10.1021/nl9034384 (2010).
100 Khoo, K. H., Chen, Y., Li, S. & Quek, S. Y. Length dependence of electron transport through molecular wires - a first principles perspective. *Physical Chemistry Chemical Physics* **17**, 77-96, doi:10.1039/C4CP05006A (2015).
101 Rurali, R. & Cartoixà, X. Theory of Defects in One-Dimensional Systems: Application to Al-Catalyzed Si Nanowires. *Nano Letters* **9**, 975-979, doi:10.1021/nl802847p (2009).
102 Buckeridge, J. *et al.* One-dimensional embedded cluster approach to modeling CdS nanowires. *Journal of Chemical Physics* **139**, doi:10.1063/1.4820415 (2013).
103 Wang, Z., Li, J., Gao, F. & Weber, W. J. Defects in gallium nitride nanowires: First principles calculations. *Journal of Applied Physics* **108**, 044305, doi:doi:http://dx.doi.org/10.1063/1.3476280 (2010).
104 Wrasse, E. O., Venezuela, P. & Baierle, R. J. Ab initio study of point defects in PbSe and PbTe: Bulk and nanowire. *Journal of Applied Physics* **116**, 183703, doi:doi:http://dx.doi.org/10.1063/1.4901640 (2014).